High-Resolution Simulations and Microphysical Validation of an Orographic Precipitation Event over the Wasatch Mountains during IPEX IOP3

BRIAN A. COLLE AND JUSTIN B. WOLFE

Institute for Terrestrial and Planetary Atmospheres, State University of New York at Stony Brook, Stony Brook, New York

W. JAMES STEENBURGH

NOAA/Cooperative Institute for Regional Prediction, and Department of Meteorology, University of Utah, Salt Lake City, Utah

DAVID E. KINGSMILL

Cooperative Institute for Research in Environmental Studies, University of Colorado, Boulder, Colorado

JUSTIN A. W. COX AND JASON C. SHAFER

NOAA/Cooperative Institute for Regional Prediction, and Department of Meteorology, University of Utah, Salt Lake City, Utah

(Manuscript received 17 November 2004, in final form 17 March 2005)

ABSTRACT

This paper investigates the kinematic flow and precipitation evolution of a winter storm over and upstream of the Wasatch Mountains [Intermountain Precipitation Experiment third intensive observing period (IPEX IOP3)] using a multiply nested version of the fifth-generation Pennsylvania State University (PSU)—National Center for Atmospheric Research (NCAR) Mesoscale Model (MM5). Validation using in situ aircraft data, radiosondes, ground-based radar, and surface observations showed that the MM5, which featured four domains with 36-, 12-, 4-, and 1.33-km grid spacing, realistically simulated the observed partial blocking of the 8–12 m s^{-1} ambient southwesterly flow and development of a convergence zone and enhanced lowland precipitation region upwind of the initial Wasatch slope. The MM5 also properly simulated the advance of this convergence zone toward the base of the Wasatch during the passage of a midlevel trough, despite not fully capturing the westerly wind shift accompanying the trough.

Accurate simulation of the observed precipitation over the central Wasatch Mountains (within 25% of observed at all stations) required a horizontal grid spacing of 1.33 km. Despite close agreement with the observed surface precipitation, the Reisner2 bulk microphysical scheme produced too much supercooled cloud water and too little snow aloft. A model microphysical budget revealed that the Reisner2 generated over half of the surface precipitation through riming and accretion, rather than snow deposition and aggregation as implied by the observations. Using an intercept for the snow size distribution that allows for greater snow concentrations aloft improved the snow predictions and reduced the cloud water overprediction.

Sensitivity studies illustrate that the reduced surface drag of the Great Salt Lake (GSL) enhanced the convergence zone and associated lowland precipitation enhancement upstream of the Wasatch Mountains. The presence of mountain ranges south of the Great Salt Lake appears to have weakened the along-barrier flow and windward convergence, resulting in a slight decrease in windward precipitation enhancement. Diabatic cooling from falling precipitation was also important for maintaining the blocked flow.

1. Introduction

During the past several years the development of new observational tools and high-resolution modeling has sparked renewed interest and field studies on orographic precipitation. This research has been motivated by 1) known deficiencies in model bulk microphysical parameterizations (Garvert et al. 2005b; Colle et al. 2005), 2) limited understanding of how the moist dynamical flows over terrain impact precipitation production (Jiang 2003; Colle 2004), and 3) limited knowledge of the microphysical processes over different geographic locations and ambient conditions.

Corresponding author address: Dr. B. A. Colle, Marine Sciences Research Center, The University at Stony Brook, State University of New York, Stony Brook, NY 11794-5000.
E-mail: bcolle@notes.cc.sunysb.edu

Progress in these areas requires detailed observations from many different locations and barrier dimensions. As a result, during the late 1990s and early 2000s, numerous field studies were designed to collect surface and aircraft data in order to better understand orographic precipitation processes and microphysics, such as the Mesoscale Alpine Project (MAP) over the European Alps during the fall of 1999 (Bougeault et al. 2001), the California Landfalling Jets Experiment (CALJET) in the winter of 1998 (Ralph et al. 1999), the Improvement of Microphysical Parameterization through Observational Verification Experiment (IMPROVE-2) over the Oregon Cascades during December 2001 (Stoelinga et al. 2003), and the Intermountain Precipitation Experiment (IPEX) over the Wasatch Mountains of Utah during February 2000 (Schultz et al. 2002). These field studies provide data from a spectrum of barrier widths, ranging from the large Alpine terrain for MAP to the moderately wide Cascades during IMPROVE-2 and the narrow (<10 km half-width) Wasatch in IPEX. In addition, the results from IMPROVE-2 and CALJET over a coastal maritime environment can be contrasted with the more continental IPEX environment that likely has more cloud condensation nuclei and less moisture availability.

For relatively stable flow cases over the Alps and Cascades, the near-surface flow decelerates, resulting in a layer of strong wind shear within 1 km of the surface (Medina et al. 2005). Turbulent vertical motions of about 1–2 $m\,s^{-1}$ within this shear layer may enhance snow aggregate growth above the freezing level (Houze and Medina 2005). The amount of upward motion and riming over the windward peaks is largest when the topographic blocking is small (Medina and Houze 2003). For example, during the partially blocked 13–14 December 2001 IMPROVE-2 case, riming was observed aloft over the windward slopes of the Cascades (Woods et al. 2005), and it was shown to be important in the observed and simulated microphysical budgets (Woods et al. 2005; Colle et al. 2005). Unblocked flow produces large rainfall events along the steep windward slopes of the California coast (Neiman et al. 2002), where orographic precipitation is best correlated with the flow below crest level when the flow is unblocked.

Although high-resolution mesoscale models can realistically simulate the kinematic flow patterns over these barriers, such as partial flow blocking and gravity waves over the Cascades (Garvert et al. 2005a), recent verification of bulk microphysical parameterizations (BMPs) has revealed large deficiencies for orographic precipitation (Colle and Zeng 2004a; Garvert et al. 2005a). Using in situ aircraft data from the 13–14 December 2001 IMPROVE-2 event and the fifth-generation Pennsylvania State University (PSU)–National Center for Atmospheric Research (NCAR) Mesoscale Model (MM5) (Grell et al. 1994), Garvert et al. (2005b) showed that the most sophisticated BMP (Reisner2) (Thompson et al. 2004) in MM5 produced too much snow aloft, thus resulting in surface precipitation overpredictions over the windward slopes and in the immediate lee of the crest. Colle et al. (2005) showed that the surface precipitation for this event was sensitive to BMP parameters such as the intercept for the snow size distribution. In particular, they showed that the fixed intercept formulation used in many BMPs (Lin et al. 1983; Rutledge and Hobbs 1983) overproduces snow and depletes too much cloud water over the crest. Other studies have utilized versions of Lin et al. (1983) and Rutledge and Hobbs (1983) to explore model microphysical sensitivities associated with convection (Gilmore et al. 2004) and hurricanes (McFarquhar and Black 2004), so the results from orographic field studies, such as IMPROVE-2, are relevant to the broader community's effort to address deficiencies in quantitative precipitation forecasting. It is clear that all BMPs suffer from uncertainties regarding particle size distributions, fall speeds, ice initiation, and autoconversions. Further information regarding some of the microphysical uncertainties shared between Reisner2 and other BMPs are highlighted in appendix A of Stoelinga et al. (2003).

The modeling results from the wider barriers of IMPROVE-2 and MAP need to be compared with narrower barriers and different ambient conditions. Using two-dimensional idealized simulations, Colle (2004) illustrated that gravity waves induced by relatively wide barriers (>30 km half-width) can generate a windward pressure perturbation and upward motion aloft that results in ice/snow aloft upstream of the barrier. Colle and Zeng (2004b) showed that the microphysical sensitivities can be different between a relatively wide barrier (>25 km half-width) and a narrower mountain of similar height. A steeper slope generates stronger vertical motion, while a smaller mountain half-width has a shorter time scale for microphysical growth. They showed that simulations over a narrow barrier with a steep slope may be more sensitive to cloud water autoconversion thresholds and the density of graupel than simulations over a wider and less steep barrier. In contrast, a wider mountain is more sensitive to snow intercepts and hydrometeor fall speeds. Overall, there have been fewer high-resolution simulations of orographic precipitation for interior mountain ranges of the Intermountain West. As a result, there has been limited veri-

fication of bulk microphysical parameterizations over these relatively narrow barriers.

The IPEX field experiment offers an opportunity to investigate orographic precipitation mechanisms and microphysical processes over the relatively narrow (<10 km half-width) Wasatch Mountains of northern Utah (Schultz et al. 2002). These microphysical results can be compared with other field studies such as IMPROVE-2. Operational models cannot resolve the steep Wasatch Front; therefore, unlike wider barriers, such as the Cascades, in which 12-km grid spacing has been shown to be sufficient for mesoscale modeling (Mass et al. 2002), the Wasatch may require at least 4-km grid spacing to generate a realistic precipitation forecast (Hart et al. 2004).

Shafer et al. (2005, manuscript submitted to *Mon. Wea. Rev.*, hereafter SSC) described the synoptic flow and development of a midlevel trough during the third intensive observing period (IOP3) of IPEX. Meanwhile, Cox et al. (2005) presented the observed kinematic and precipitation structures of IOP3 using conventional data, in situ airborne data from the National Oceanic and Atmospheric Administration (NOAA) WP-3D, and two University of Oklahoma Doppler on Wheels (DOW) X-band radars (Wurman et al. 1997), which were located 20 km upstream of the Wasatch. Over 80 cm of snow fell near the Wasatch crest during IOP3, which was the largest precipitation event during IPEX. Cox et al. (2005) showed using Doppler winds that the near-surface flow was blocked by the Wasatch, resulting in convergent near-surface flow 20–40 km upstream of the Wasatch between the upstream southwesterlies and the along-barrier southerly flow. The upstream convergence resulted in enhanced precipitation over the region of blocked flow and windward slope, while cross-barrier flow at crest level resulted in significant spillover over the crest and a lee wave.

Field observations alone cannot answer some fundamental issues regarding the mesoscale evolution of this IPEX event; therefore, this paper extends the observational work of Cox et al. (2005) by completing a series of high-resolution model simulations of IPEX IOP3. The purpose of this paper is fourfold: 1) to use the MM5 to better understand the three-dimensional flow and precipitation evolution around the Wasatch, 2) to verify the MM5 precipitation forecasts with decreasing horizontal grid spacing, 3) to validate the model microphysics over a relatively narrow mountain barrier (i.e., the Wasatch Mountains) using aircraft data and a model microphysical budget, and 4) to determine the processes responsible for the formation of the windward convergence zone and precipitation region.

Section 2 provides a detailed description of the model, experimental design, and analysis methods. Section 3 presents the model synoptic and mesoscale evolution of the event and comparison with observations. The in situ microphysical verification, microphysical budget, and microphysical sensitivity simulations are presented in section 4. Section 5 includes a discussion on the impact of the upstream terrain, Great Salt Lake (GSL), and diabatic cooling from precipitation on the upstream blocking and precipitation evolution. Summary and conclusions are presented in section 6.

2. Data and analysis methods

The MM5 (version 3.5) was used in nonhydrostatic mode to simulate IOP3 and to provide additional sensitivity simulations. For this simulation, stationary 1.33-, 4-, and 12-km domains were nested within a 36-km domain using one-way nest interfaces (Fig. 1a). The model top was set at 100 mb. Thirty-seven unevenly spaced full-sigma levels were used in the vertical, with seven levels in the boundary layer. Five-minute-averaged terrain data were analyzed to the 36- and 12-km model grids using a Cressman analysis scheme and filtered by a two-pass smoother/desmoother. For the 4- and 1.33-km domains (Fig. 1b), a 30-s topography dataset was interpolated to the grid in order to better resolve the inland hills and valleys. A 30-s land-use dataset from NCAR was used to initialize 24 surface categories for all domains. Initial atmospheric conditions at 1200 UTC 12 February 2000 were generated by interpolating the National Centers for Environmental Prediction (NCEP) Global Forecast System (GFS) model analysis (1° resolution) to the MM5 grid. The 6-hourly GFS analyses were linearly interpolated in time in order to provide the evolving lateral boundary conditions for the 36-km domain. The U.S. Navy Optimum Thermal Interpolation System (OTIS) sea surface temperature analyses (~30 km grid spacing) were used to initialize the MM5 surface temperatures over water. The Great Salt Lake temperature was set to 6°C, as observed at the Hat Island Mesowest site maintained by the University of Utah (Fig. 1b). The Grell convective parameterization (Grell et al. 1994) was applied, except for the 4- and 1.33-km domains, where convective processes were resolved explicitly. The planetary boundary layer (PBL) was parameterized using NCEP's Medium-Range Forecast (MRF) scheme (Hong and Pan 1996). Klemp and Durran's (1983) upper-radiative boundary condition was applied in order to prevent gravity waves from being reflected off the model top.

The control (CTL) simulation used the Reisner2 ex-

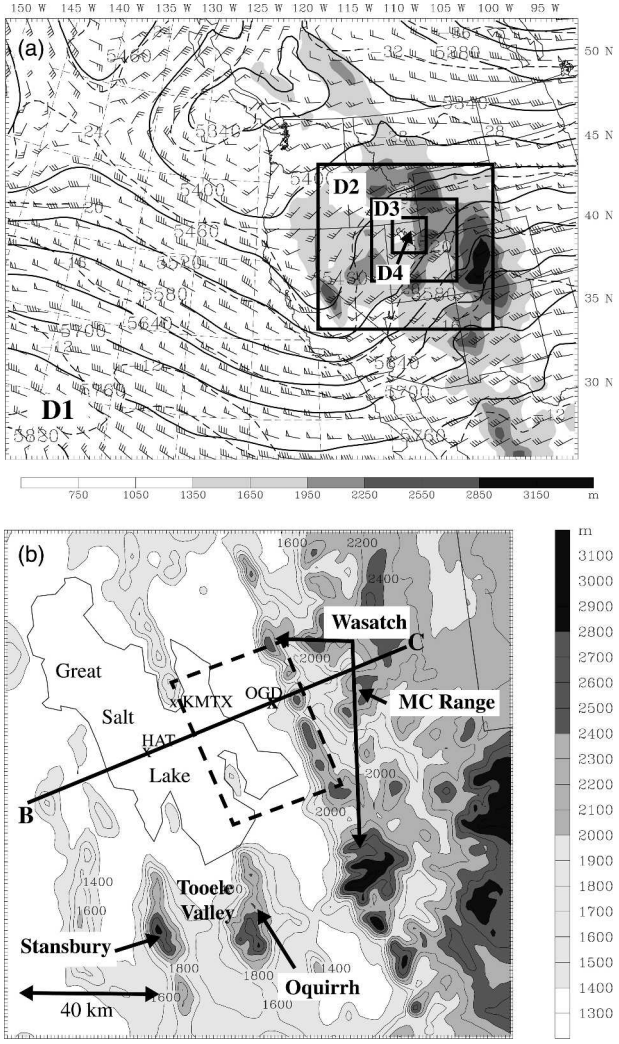

FIG. 1. (a) The 500-mb geopotential height (solid) every 60 m, temperature (dashed every 4°C), and wind barbs (full barb = 10 kt) at 0000 UTC 12 Feb 2000 (0 h) for the 36-km domain. The inner boxes (D2, D3, and D4) show the location of the 12-, 4-, and 1.33-km nested domains. Model terrain is contoured and shaded every 100 m for the 36-km domain. (b) Model terrain contoured every 200 m and shaded for the 1.33-km domain. Line segment BC is the P-3 flight track over the Wasatch, and the dashed box shows the region where the average microphysical budget was calculated in the model.

plicit moisture scheme from version 3.6 of the MM5 (Reisner et al. 1998; Thompson et al. 2004). To determine which microphysical processes contributed most to the production and depletion of a specific hydrometeor category, a model microphysical budget for a volume upstream of the Wasatch was calculated for a given period using the approach outlined in Colle and Zeng (2004a). The relative importance of each process in moving water mass is quantified by normalizing each process in the appendix with the integrated water vapor loss within that same box. This is accomplished using

$$\overline{P_{qqqq}} = \frac{\sum_{i,j,k} p^*(i,j) \times P_{qqqq}(i,j,k) \times \Delta\sigma(k)}{\sum_{i,j,k} p^*(i,j) \times \mathrm{WVL}(i,j,k) \times \Delta\sigma(k)}, \quad (1)$$

where P_{qqqq} (i, j, k) is the conversion rate of a specific microphysical process averaged for the two adjacent sigma levels, WVL is the total water vapor loss rate from microphysical processes within the box, and $\Delta\sigma$ is the sigma-level difference.

3. Synoptic and mesoscale evolution

SSC and Cox et al. (2005) provide the observational large-scale and mesoscale analysis of IPEX IOP3, respectively; therefore, only limited observations are presented below in order to provide context for the MM5 simulations.

a. Synoptic overview

At 1200 UTC 12 February 2000, which is about 5 h before the NOAA P-3 aircraft began collecting data over the Wasatch, a 500-mb short-wave trough extended from the Pacific Northwest southward toward southern California, while a short-wave ridge was situated to the east over the Rocky Mountains (Fig. 1a). During the 6-h IOP3 period (1800 UTC 12 February–0000 UTC 13 February 2000), there was a midlevel (700–600 mb) trough that crossed the IOP area a few hours before the 500-mb and surface-based trough passages (see SSC for details), resulting in a wind shift from southwesterly to west–northwesterly between 700 and 600 mb (just above the Wasatch crest) around 2100 UTC 12 February. This midlevel trough passage was apparent in the observed Ogden, Utah, sounding (for location see OGD in Fig. 1b) between 1800 and 2100 UTC 12 February (Figs. 2a,c). At 1800 UTC (Fig. 2a), there was generally southwesterly flow 7–12 m s^{-1} between 700 and 600 mb, with the winds veering to more westerly around 10 m s^{-1} by 2100 UTC (Fig. 2c). This trough was not associated with any significant temperature or moisture change aloft. None of the NCEP operational models or the MM5 could properly simulate the intensity of this trough passage (Figs. 2b,d), with the MM5 winds veering only slightly more southwesterly around 750 mb between 1800 and 2100 UTC.

Figure 3 shows the surface winds and the pressure at 1500 m above mean sea level (MSL) from the 12-km MM5 domain. The 1500-m level was chosen since it provides a better estimate of the pressure gradient than

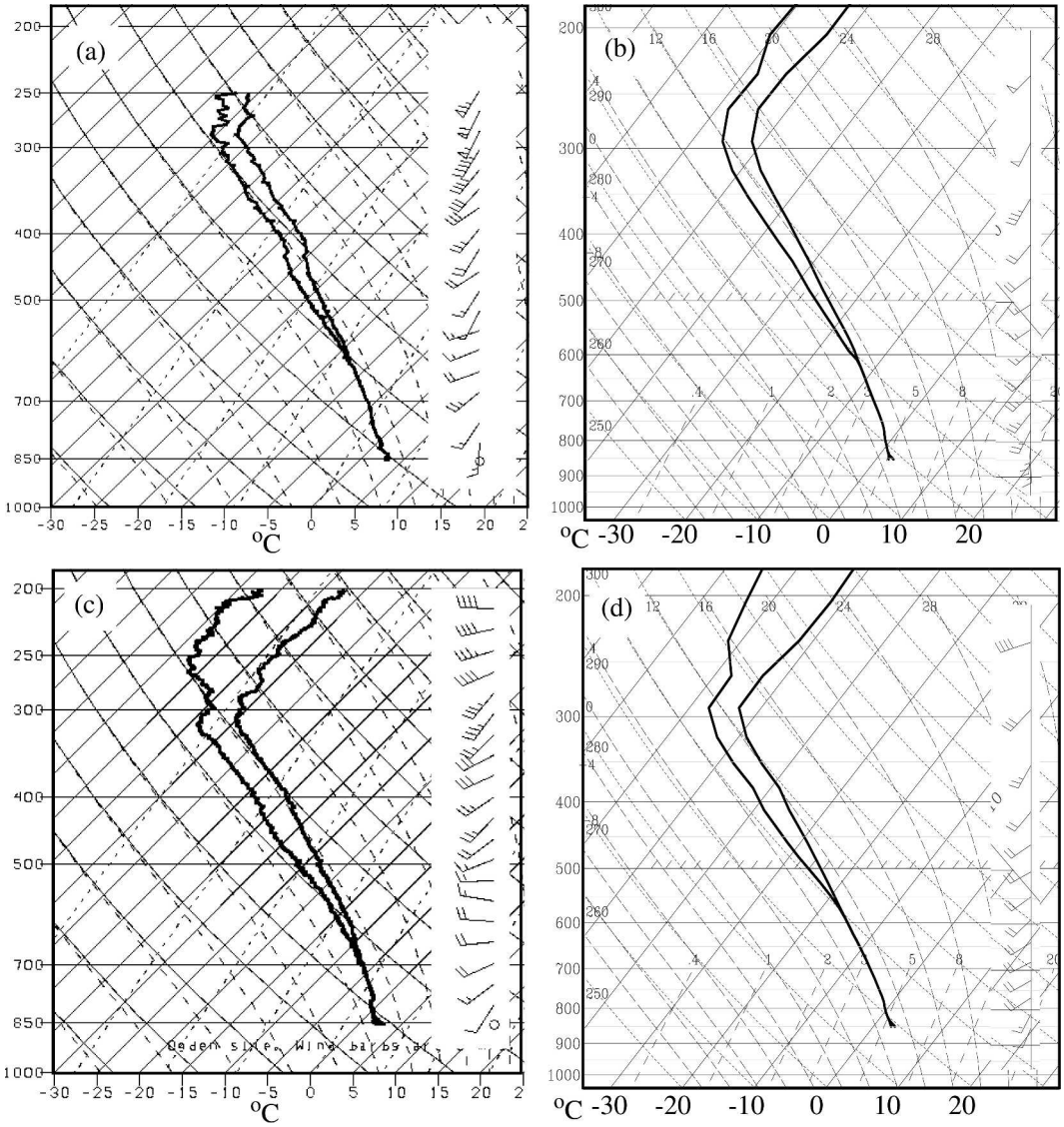

FIG. 2. (a) Observed sounding at Ogden, UT (see OGD in Fig. 1b for location), at 1730 UTC 12 Feb showing temperature, dewpoint, and winds (1 full barb = 10 kt) on a skew-*T* chart. (b) Same as (a) except for the 1.33-km MM5 simulation at hour 6. (c) Same as (a) except for 2035 UTC 12 Feb. (d) Same as (b) except for hour 9 of the simulation.

a conventional sea level pressure analysis over high terrain. At 1800 UTC 12 February 2000 (Fig. 3a), the surface baroclinic trough over southeast Idaho extended southwestward to just west of the GSL, which was 50 km to the east of the observed location (SSC). The surface winds shifted from south–southwesterly ahead of the trough near the Wasatch to westerly over Nevada. By 0000 UTC 13 February (Fig. 3b), the simulated surface trough had crossed the Wasatch Front, and the surface flow was primarily westerly at 5–7 m s^{-1} across much of northern Utah. The simulated trough was close to the observed shown in SSC. The west–northwesterly winds extended throughout the troposphere in both the model and observed as the 500-mb trough had crossed the region (not shown).

b. Mesoscale overview

At 1800 UTC 12 February (Fig. 4a), there was observed southwesterly flow over the GSL and to the west, with more southerly flow channeling within the Tooele and Salt Lake Valleys to the south. Meanwhile, there was terrain-parallel southerly flow adjacent to the Wasatch as a result of flow blocking, which resulted in a low-level convergence 20 km upstream of the Wa-

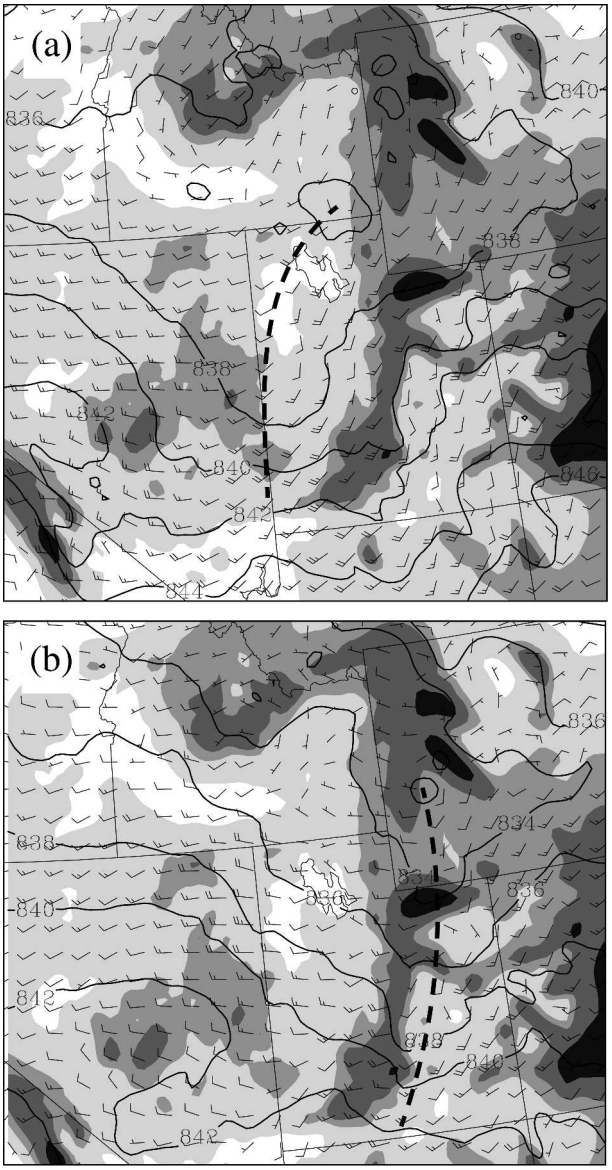

FIG. 3. (a) Pressure (solid every 2 mb) at 1500 m MSL and surface winds (1 full barb = 10 kt) at 1800 UTC 12 Feb from the 12-km MM5 (hour 6). The 12-km terrain is shaded using the scale in Fig. 1a. (b) Same as (a) except for 0000 UTC 13 Feb 2000. The dashed line represents the pressure trough axis at 1500 m MSL.

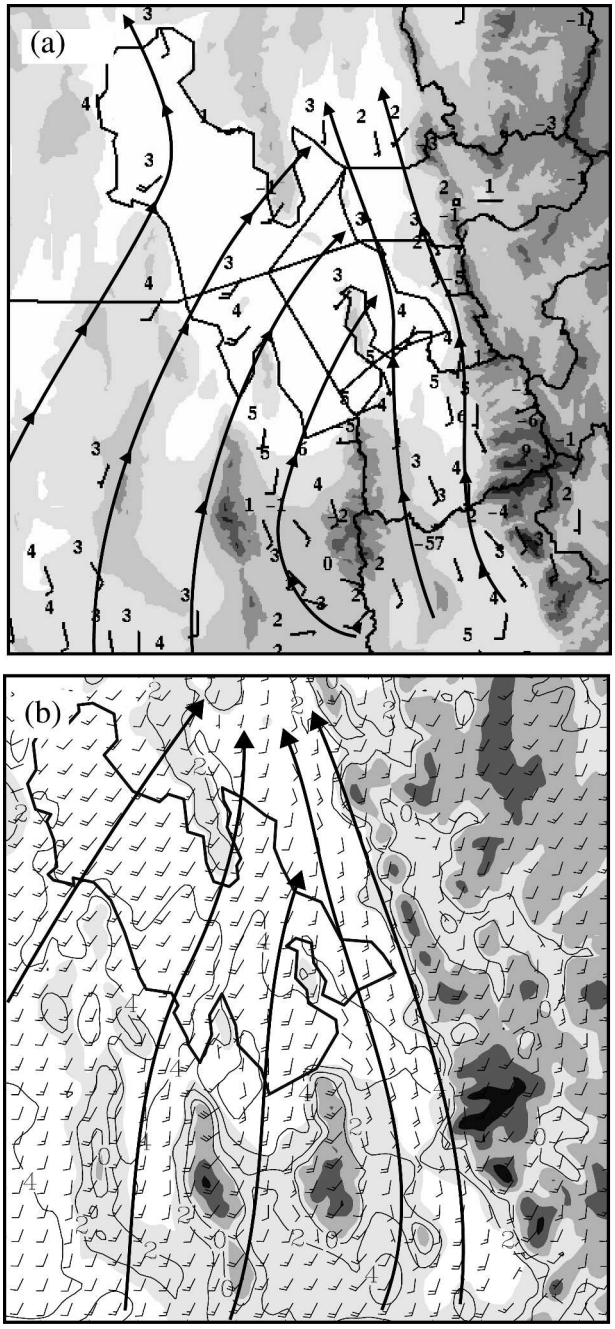

FIG. 4. (a) Observed surface winds (full barb = 10 kt), surface streamlines, and temperatures in °C at 1800 UTC 12 Feb. (b) Simulated surface winds, temperatures (solid every 2°C), and streamlines at 1800 UTC 12 Feb (hour 6). Terrain is shaded for reference.

satch. The MM5 at 1.33-km grid spacing realistically simulated the terrain-channeled flow and convergence upstream of the Wasatch (Fig. 4b). As observed, the model surface temperatures decreased from around 4°C over the lowlands to the southeast of the Salt Lake to 2°–3°C just northeast of the lake. This suggests that there was some diabatic cooling from precipitation as the surface air parcels advected northward along the barrier. The low-level blocked flow was evident in the OGD sounding in the model and observed at this time as the low-level southerly flow near the surface veered to south-southwesterly by 750 mb (Figs. 2a,b).

Figure 5 compares the observed precipitation structures from both the KMTX Weather Surveillance Radar-1988 Doppler (WSR-88D) and the NOAA P-3 tail

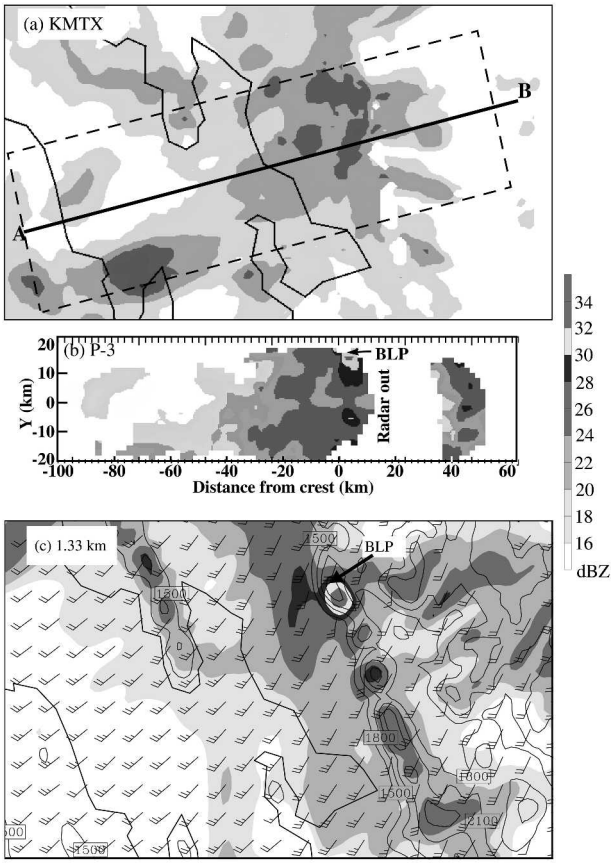

FIG. 5. (a) KMTX reflectivity (2600 m MSL) at 1830 UTC 12 Feb 2000. (b) P-3 tail radar reflectivity (2640 m MSL) collected from 1817 to 1835 UTC 12 Feb 2000 [location denoted by the dashed box in (a)]. The location of Ben Lomond peak is given by BLP. (c) Simulated reflectivity and winds at 2600 m from the 1.33-km domain at 1830 UTC 12 Feb. Line segment AB is the location of the P-3 stacks and model cross section in Fig. 6.

radar at 2600 m MSL for 1830 UTC 12 February with the model-derived reflectivities and winds at this same altitude.[1] Both the model and observed had a region of enhanced precipitation extending 30 km to the west of the Wasatch crest. The leading edge of the precipitation enhancement (to 26 dBZ) was collocated with the low-level flow convergence between the southwesterlies upstream and southerlies near the barrier (Fig. 4). The maximum model and observed reflectivities (35 dBZ) were over the southern windward slope of Ben Lomond peak (Figs. 5b,c), which was orientated more normal to the south–southwesterly flow at 2.6 km (Fig. 5c). The model underpredicted the spatial extent of the precipitation upstream over the GSL, and it was unable to simulate the transient area of moderate precipitation observed near the northern Stansbury Mountains.

Cross section AB taken across the Wasatch at 1800 UTC compares the simulated and observed reflectivity structures and winds normal to the barrier (Figs. 6a,b). Observed reflectivities were derived by the NOAA P-3 tail radar, while the DOW radar and in situ NOAA P-3 data were used to obtain the winds in the section (Cox et al. 2005). The cross-barrier flow in the model increased with height from 4–6 m s^{-1} near the surface to a maximum of 10–12 m s^{-1} at 3 km MSL about 40 km upwind at the Wasatch, which was 1–2 m s^{-1} weaker than observed. Flow blocking within 30 km of the Wasatch resulted in a horizontal gradient in cross-barrier flow between the surface and 2.6 km MSL. At the leading edge of the blocked flow there was more rapid ascent and a sharp increase in reflectivity in both the model and observations. Above this blocked flow at 2.6 km MSL there was 12 m s^{-1} cross-barrier flow, which resulted in a precipitation maximum near the crest as

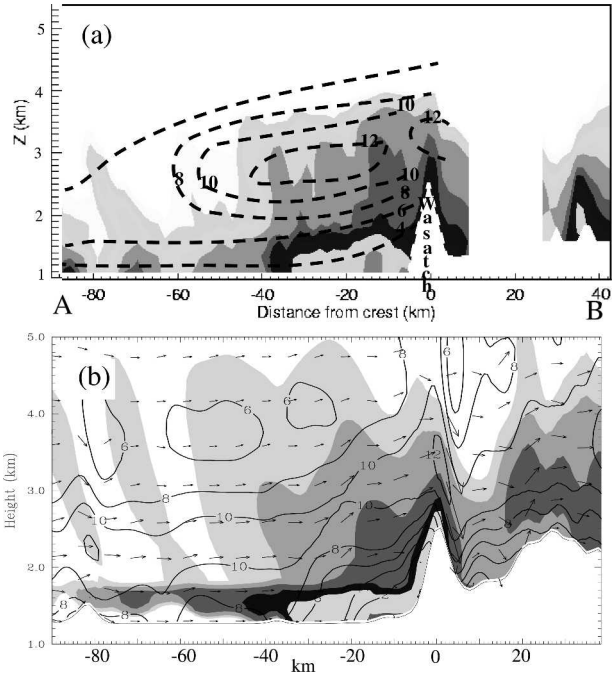

FIG. 6. (a) NOAA P-3 tail radar reflectivities (shaded every 2 dBZ using the scale on Fig. 5) and cross-barrier wind speed derived from the DOW radars and NOAA P-3 in situ data (dashed every 2 m s^{-1}) at 1800 UTC 12 Feb along section AB in Fig. 5. (b) Same as (a) except showing the simulated reflectivity, wind circulation in cross section AB, and wind speed parallel to the section (solid every 2 m s^{-1}).

[1] The synthesis of the NOAA P-3 tail radar is described in Cox et al. (2005). The model-based reflectivities were calculated using empirical relations based on the model cloud and precipitation mixing ratios (Fovell and Ogura 1988). To make this approach consistent with the Reisner2 (Thompson) scheme, a variable intercept for the snow size distribution that is a function of temperature was used.

shown in Cox et al. (2005). There was significant cross-barrier flow over the upper windward slope and crest, resulting in significant spillover of precipitation over the crest and significant leeside subsidence and drying aloft.

As noted by Cox et al. (2005), there were no significant changes in the observed kinematic and cloud structures around the Wasatch between 1800 and 1945 UTC 12 February, but larger changes were evident by 2100 UTC. By this time there was a deeper layer of strong (>10 m s^{-1}) cross-barrier flow between 2 and 3 km MSL (see Figs. 8 and 15 of Cox et al. 2005), while a shallow mixed layer developed 50–100 km upstream of the barrier (Cox et al. 2005). As a result, the observed Froude number ($Fr = U/h_mN$) below crest level increased from 0.5 to 0.75, and a similar increase occurred in the model given the slight decrease in average stability below 800 mb and the increase in cross-barrier (west-southwesterly) flow around crest level (750 mb) at OGD at 2100 UTC (Fig. 2c). In addition, by 2100 UTC the reverse shear profile above crest level had weakened, which has been shown in previous two-dimensional modeling studies to favor a shallower windward pressure perturbation and upward motion over the windward slope (Colle 2004).

These changes in ambient conditions resulted in reduced blocking upstream of the Wasatch by 2100 UTC. The convergence between southerly and southwesterly flow near the surface advanced toward the barrier by this time (Fig. 7a), with the model 10 km farther east than the observations (not shown). The migration of the convergence line toward the barrier was less pronounced to the south in both the model and observations, resulting in the line having a 10°–20° orientation toward the northern Wasatch. Cross section AB illustrates that the depth of the terrain-normal flow deceleration was limited to below 2 km upstream of the crest by 2100 UTC (Fig. 8a). As a result, there was greater cross-barrier flow over the upper windward slope, resulting in heavier precipitation over the crest as compared to 3 h earlier and larger amounts of spillover of precipitation along the lee slope, which was also observed by the NOAA P-3 aircraft at this time (see Fig. 13 of Cox et al. 2005). The western edge of the heaviest precipitation had migrated toward the barrier by 2100 UTC (Fig. 9a), with the precipitation rates increasing over the Wasatch crest. However, the heaviest precipitation was still located along the southern slopes of Ben Lomond peak.

At 0000 UTC 13 February (Fig. 7b), the surface flow had become more westerly over the Great Salt Lake and there was little evidence of terrain-parallel southerlies along the Wasatch to the east of the lake. By this time the temperatures at around 600 mb had dropped by about 1°–2°C, resulting in a nearly moist adiabatic lapse rate from the surface to midlevels at OGD (not shown), with the exception of a weak stable layer between 800 and 775 mb. The low-level Froude number was greater than one by this time in the model and observations (not shown), thus favoring less flow blocking.

For cross section AB at 0000 UTC (Fig. 8b), there was flow deceleration near the Wasatch. The heaviest precipitation aloft had shifted to the east of the Wa-

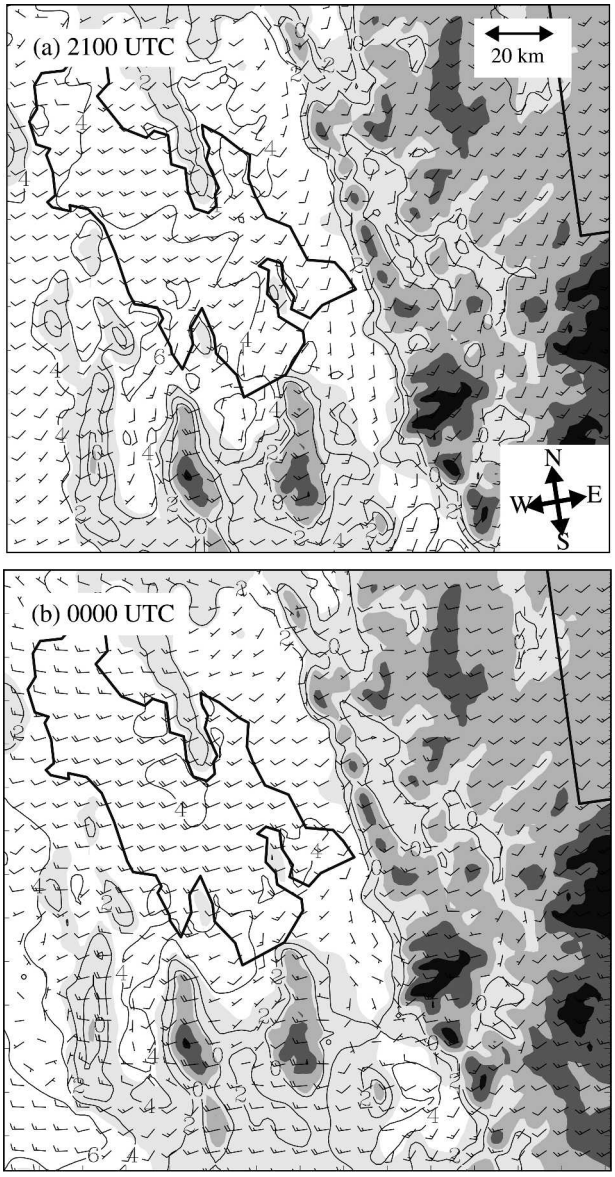

FIG. 7. (a) Simulated surface winds (full barb = 10 kt) and temperatures (solid every 2°C) at 2100 UTC 12 Feb (hour 9) from the 1.33-km domain. Terrain is shaded for reference using the scale in Fig. 1b. (b) Same as (a) except for 0000 UTC 13 Feb 2000.

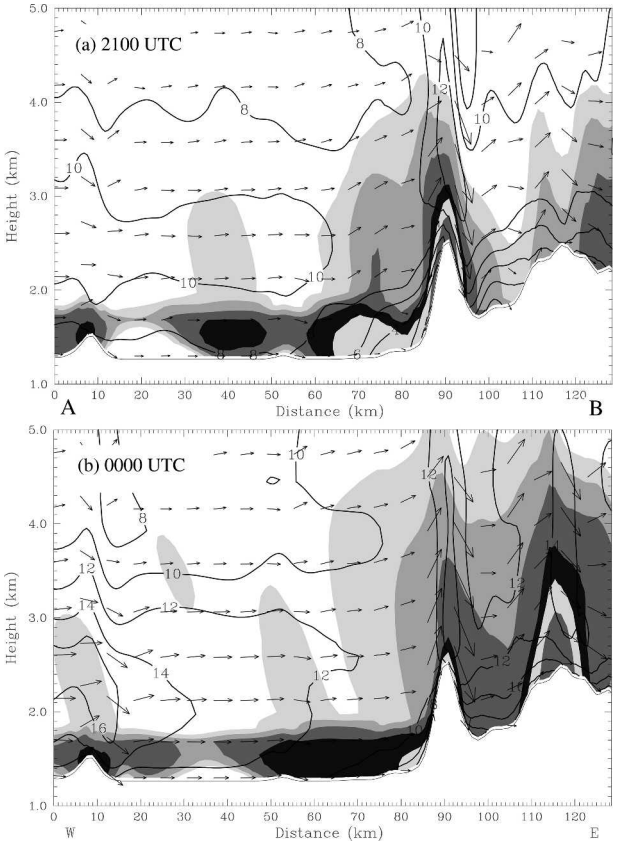

FIG. 8. Simulated reflectivity (shaded in dBZ using the scale in Fig. 5) for cross section AB, wind vector circulation along the section, and wind speed parallel to the section (solid every 2 m s^{-1}) at (a) 2100 UTC 12 Feb and (b) 0000 UTC 13 Feb. The location of AB is shown in Fig. 5.

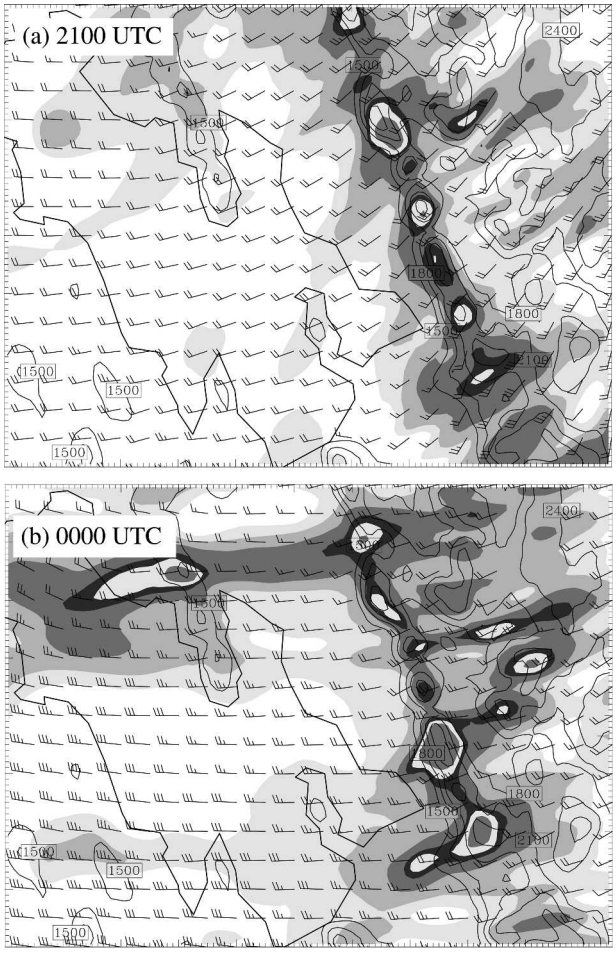

FIG. 9. Simulated reflectivity and winds at 2600 m MSL from the 1.33-km domain at (a) 2100 UTC 12 Feb and (b) 0000 UTC 13 Feb 2000.

satch, with significant spillover over the lee and upslope flow over the Monte Cristo Range to the east (MC Range on Fig. 1b). The vertical gradient of dBZ still existed below 1.8 km MSL upstream of the Wasatch as a result of snow melting and warm-rain processes (cloud water accretion) within the boundary layer. At crest level (2.6 km MSL), there was also westerly flow across the region (Fig. 9b), and much less precipitation enhancement upstream of the Wasatch as compared to 3–6 h earlier. The heaviest precipitation had shifted to some of the higher Wasatch peaks to the south with the stronger upslope flow. The precipitation over southeastern Ben Lomond peak had weakened as the flow turned more westerly with the midlevel trough, suggesting that this maximum earlier in the event was tied to more southerly flow ahead of the trough.

Figure 10a shows the 6-h precipitation for the 1.33-km domain between 1800 UTC 12 February and 0000 UTC 13 February, the simulated percent of observed precipitation at the available gauge locations, and the surface winds at 1800 UTC. As observed (see Fig. 2 of Cox et al. 2005), the 1.33-km simulation produced a sharp gradient in 6-h precipitation 10–15 km upstream of the Wasatch as a result of the upstream flow blocking. The heaviest precipitation was generally located near the Wasatch crest, with the greatest (28 mm) near Ben Lomond peak, similar to the observed. Meanwhile, as observed, there was little or no precipitation to the west over the central and western Salt Lake. Over the central Wasatch near OGD, the model was generally within 25% of the observed at all stations, while there was significant (>30%) underprediction well upstream of the Wasatch. In contrast, there was overprediction (by 50%–100%) in the immediate lee of the higher and wider southern Wasatch Front as well as the Monte Cristo range to the east of the northern Wasatch.

At 4-km grid spacing (Fig. 10b), the Wasatch cannot be resolved as a narrow ridge; rather, the 4 km has a relatively steep windward slope extending to a broader

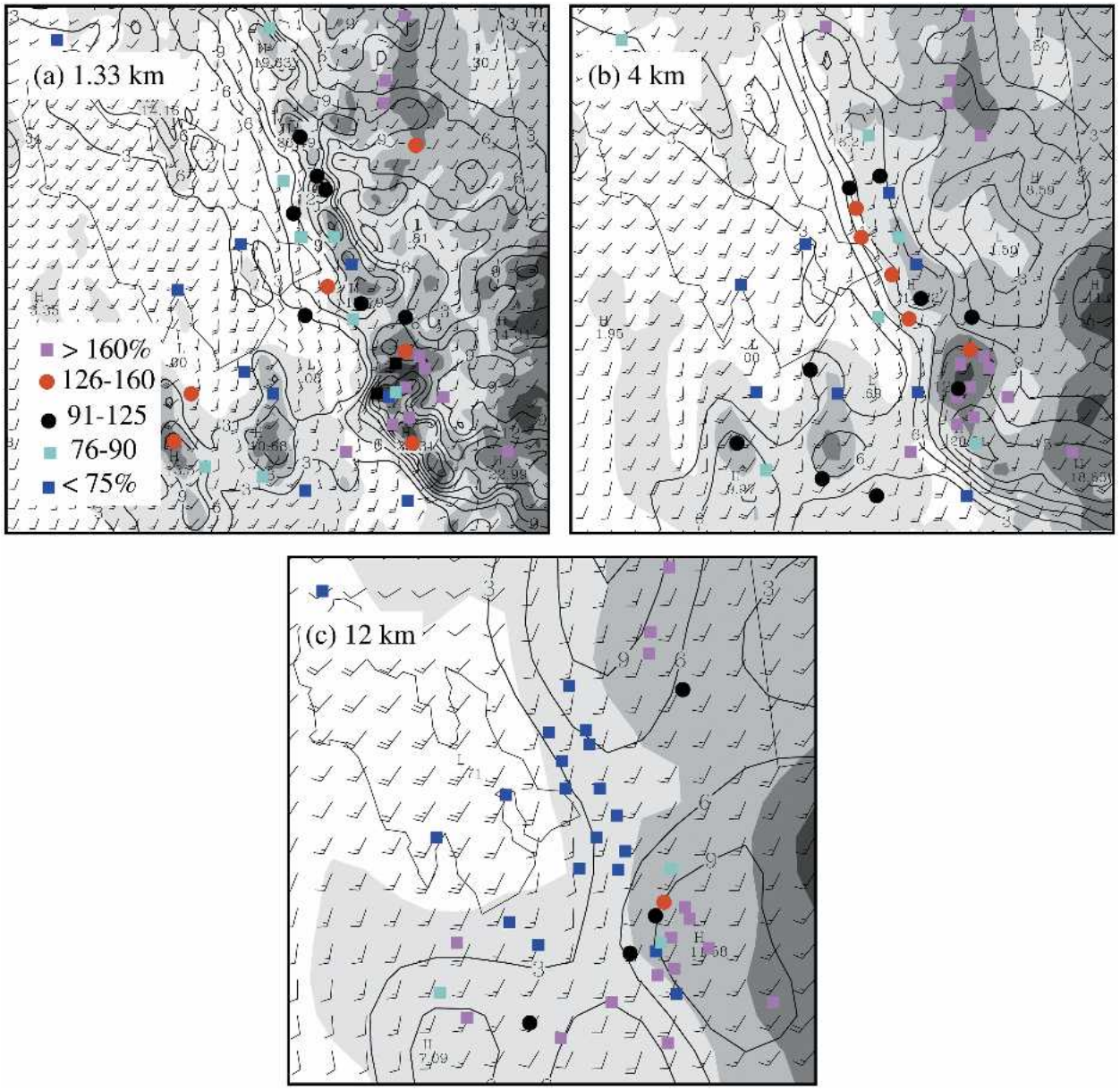

FIG. 10. (a) Total precipitation (solid every 3 mm) for the 1.33-km domain from 1800 UTC 12 Feb to 0000 UTC 13 Feb. The percent of observed precipitation at each gauge site for 1800–0000 UTC is color-coded using the inset scale. The 1.33-km terrain is shaded using the scale in Fig. 1b, and the surface winds at 1800 UTC 12 Feb are shown for reference (full barb = 10 kt). (b) Same simulation as (a) except for 4-km grid spacing. (c) Same as (a) except for 12-km grid spacing.

plateau. However, the 4-km simulation was still able to simulate the development of nearly terrain-parallel flow and convergence upstream of the Wasatch at 1800 UTC 12 February. As a result of the smoother terrain in the 4-km domain, the 4 km has a few more locations, with 20%–30% underprediction over the central Wasatch than the 1.33 km. The 4-km slope also extends farther upwind (west) than reality, resulting in excessive upslope flow and overprediction (by 40%–60%) over some lower windward slope locations. Meanwhile, the 4-km terrain is similar to the 1.33-km Wasatch to the south, so the precipitation verification results are similar in this region.

At 12-km grid spacing (Fig. 10c), there is only a gradual slope from west to the east of the Salt Lake. This smoother slope results in much less low-level flow blocking than the 4-km domain, with little upstream convergence west of the Wasatch. As a result, the 12-

km precipitation is dramatically less immediately upstream of the Wasatch, and the 6-h precipitation over this region is less than half that of the 4-km domain, with the 12 km having less than 40% of the observed over the central and northern Wasatch and immediately upstream. In contrast, the 12-km run has more overpredictions over the lower windward slope of the wider Wasatch to the south and has overpredictions to the lee of the crest similar to the higher-resolution domains.

These precipitation verification results highlight the importance of increased horizontal resolution to resolve the upstream flow blocking and upslope flow over the Wasatch Front. There are substantial improvements in the precipitation simulation as the grid spacing was decreased from 12- to 4-km grid spacing, and only the 1.33-km domain can resolve the finescale impacts of the narrow Wasatch ridge. The large precipitation improvements from 12 to 4 km are consistent with longer-term precipitation verification results of Hart et al. (2004) over this region using the MM5. Overall, the reduction in improvement from 4 to 1.33 km over the Wasatch is similar to the lack of improvement noted from 12 to 4 km over wider barriers such as the Washington Cascades (Colle et al. 2000).

4. Microphysical evaluation

a. Verification of control run

The NOAA P-3 aircraft completed four stacks of west-southwest- to east-northeast-oriented flight legs across the central Wasatch (segment BC on Fig. 1b) over a 6-h period when the storm produced the largest amount of precipitation. These flight legs were executed at altitudes corresponding to critical air temperatures for microphysical processes ($-5°$ to $-20°$C). Several in situ sensors on the aircraft were used to make kinematic and microphysical measurements within and adjacent to the precipitating cloud. A subset of these observations is emphasized in this study. Air temperature, static pressure, horizontal wind speed, and vertical wind velocity were obtained from the standard flight-level dataset (Jorgensen 1984; Jorgensen and LeMone 1989). Cloud liquid water content was derived from a King probe (King et al. 1978). Size distributions of cloud and precipitation particles were derived from two optical array probes (Knollenberg 1970; Korolev et al. 1998a): a two-dimensional gray cloud probe (2DGC) having an array width of 1920 mm with an array resolution of 30 mm and a two-dimensional mono precipitation probe (2DP) having an array width of 6400 mm with an array resolution of 200 mm. Prior to quantitative analysis, spurious images of the types described by Heymsfield and Baumgardner (1985) were removed from the dataset. For particles entirely in the diode array of these probes, the maximum dimension of the image was used as the sizing metric. To increase the effective sample volume, partial images occulting one or both edge diodes were sized using a reconstruction technique (Heymsfield and Parrish 1978; Korolev et al. 2000). Composite size distributions for each 16-s averaging interval ($\sim$2 km of flight track) were constructed by merging 2DGC data at particle sizes less 1 mm with 2DP data at particle sizes greater than or equal to 1 mm. The choice of 1 mm for the crossover between probes was based on the fact that this was the smallest size bin where the 2DP was not obviously influenced by electronic roll-off effects (Baumgardner and Korolev 1997; Korolev et al. 1998a).

The particle imagery was reviewed carefully to infer particle types and the degree of riming. Subjective analysis indicates that most particles were of irregular shape with jagged edges and porous structures, suggestive of ice crystal aggregates with little or no riming. Mixing ratios were calculated from the size distributions by using a mass-dimension relation from Heymsfield et al. (2002), which is very similar to the one reported by Locatelli and Hobbs (1974) for aggregates of side planes, bullets, plates, and columns. Heymsfield et al. (2002) and Korolev and Strapp (2002) have performed intercomparisons of mixing ratio obtained from direct measurements (Twohy et al. 1997; Korolev et al. 1998b) with calculations from particle size distributions and have found that while large differences are possible ($\sim$100%), there is usually reasonable agreement ($\sim$20%) between the measurements.

The microphysical verification in this study is based on a stack of four flight legs across the Wasatch between 1907 and 2007 UTC 12 February (Fig. 1b). This stack was chosen since it is a representative period during the middle of the IOP, and the two later stacks occurred when the simulated cross-barrier flow was substantially more southwesterly than the observed (cf. Figs. 2c,d). Since it is imperative that the model has an accurate kinematic forecast in order to evaluate the microphysics, these later legs are not discussed quantitatively. The NOAA P-3 kinematic and cloud water data were averaged every 10 s, and the 15-min MM5 output was linearly interpolated to obtain 10-s intervals as well as the 16-s intervals for the time-averaged 2DGC/2DP data.

Figure 11 shows the cross-barrier wind (west-southwest flow) and vertical velocity versus forecast hour for the 1.33-km MM5 and the NOAA P-3 at the

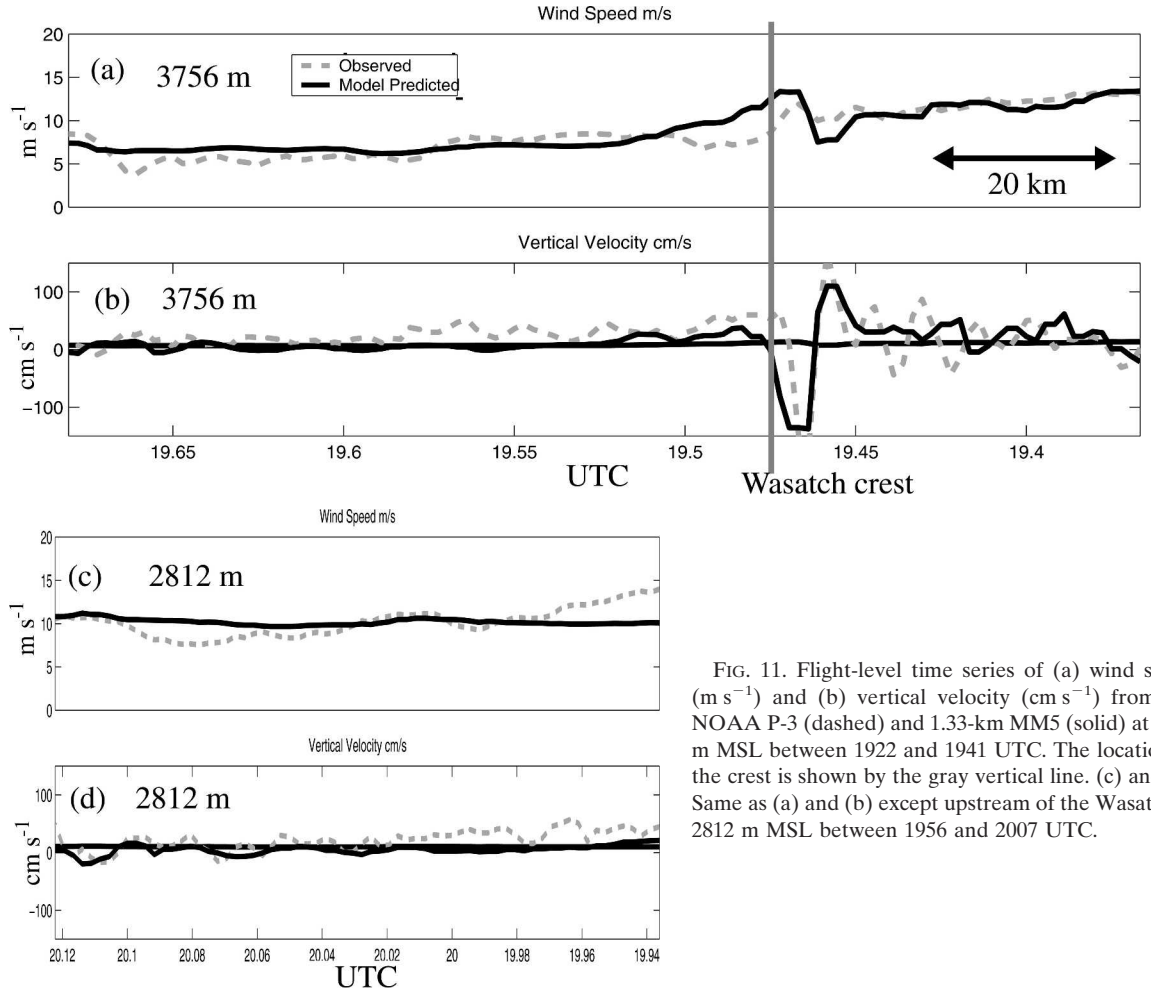

FIG. 11. Flight-level time series of (a) wind speed ($m\ s^{-1}$) and (b) vertical velocity ($cm\ s^{-1}$) from the NOAA P-3 (dashed) and 1.33-km MM5 (solid) at 3756 m MSL between 1922 and 1941 UTC. The location of the crest is shown by the gray vertical line. (c) and (d) Same as (a) and (b) except upstream of the Wasatch at 2812 m MSL between 1956 and 2007 UTC.

3756 and 2812 m. At 3756 m MSL (Figs. 11a,b), the observed cross-barrier flow was around 5 $m\ s^{-1}$ about 70 km upstream of the Wasatch, and the flow gradually increased toward the east to over 8 $m\ s^{-1}$. The model produced a similar wind increase, but the model winds were around 4 $m\ s^{-1}$ too strong over the Wasatch windward slope. This positive wind error would favor excessive spillover of precipitation into the lee of the Wasatch, but this was not obvious when comparing with the available observations (Figs. 6, 10a). The strongest vertical velocities were in the immediate lee of the Wasatch crest, where a lee wave is evinced by the oscillating pattern of downward and upward motions that have a horizontal wavelength of about 10 km. The 1.33-km MM5 could not accurately produce these wavelike fluctuations, and lee wave subsidence began slightly more upstream of the crest in the model than observed. The model upward motion was about 0.2 $m\ s^{-1}$ weaker than the observed 30–40 km upstream of the Wasatch, and this underprediction remains even after considering the uncertainty of the P-3 vertical velocity measurements of $\sim$0.1 $m\ s^{-1}$ (Jorgensen and LeMone 1989). The impact of this vertical velocity error on the model microphysics is discussed below.

Upstream of the Wasatch at 2812 m MSL (Figs. 11c,d), the cross-barrier flow was between 8 and 12 $m\ s^{-1}$ in the observations, with the model close to the observed well upstream of the barrier and 2–3 $m\ s^{-1}$ too weak 30–40 km upstream of the windward slope. The model vertical motions were slightly weaker than observed 20–50 km upstream of the barrier.

To illustrate the spatial distribution of simulated hydrometeors aloft during this stack of flight legs, Fig. 12 shows the snow, cloud water, and graupel mixing ratios from the 1.33-km MM5 for a cross section along the flight track averaged between 1900 and 2000 UTC 12 February. Most of the cloud water 40 km upstream of the barrier was located below 3 km MSL, and there was little graupel in this region. Meanwhile, there was a sharp increase in snow and cloud water below 4 km

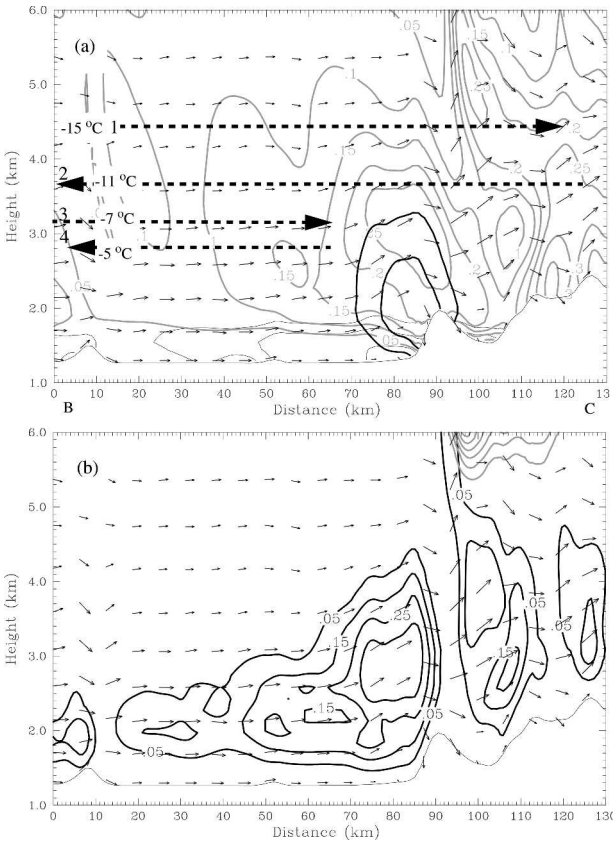

FIG. 12. Cross section along BC averaged between 1900 and 2000 UTC 12 Feb showing (a) simulated snow (gray) and graupel (bold black) every 0.05 g kg^{-1}, rain (thin black below 2 km) every 0.10 g kg^{-1}, and circulation vectors in the cross section. The NOAA P-3 flight legs during the period and temperature averaged along the flight leg are shown by the dashed lines 1–4 and inset boxes, respectively. (b) Same simulation as (a) except for cloud water (black) every 0.10 g kg^{-1} and cloud ice (gray) every 0.02 g kg^{-1}.

within 30 km of the barrier in association with the sloped ascent over the blocked flow. The snow became heavily rimed in this region, resulting in large amounts of graupel adjacent to the windward slope.

The model cloud water and snow mixing ratios are compared to the P-3 observations in Figs. 13 and 14, respectively, for the four flight legs aloft between 1900 and 2000 UTC. Graupel was not included in the comparisons, since little was observed or simulated at P-3 flight level. Furthermore, even though the model considers graupel as heavily rimed snow (density = 400 kg m^{-3}), it was not included for the snow comparisons since little riming was observed in the particle imagery. At 4356 m MSL (Fig. 13a), there was no cloud water observed by the NOAA P-3, while the MM5 generated 0.1–0.2 g kg^{-1} to the east of the Wasatch crest. The model also produced around 0.2 g kg^{-1} more snow than observed in this region as well (Fig. 14a). Meanwhile, upstream of the Wasatch, both the model and observed had no cloud water and snow amounts generally less than 0.2 g kg^{-1}. At 3756 m (Fig. 13b), some cloud water (0.1 g kg^{-1}) was observed by the NOAA P-3 over the crest, while the model produced over twice as much as observed over the windward slope and to the east of the Wasatch. Some of the excessive snow and cloud water in the model with the lee wave may be the result of too little simulated subsidence over the lee slope (Fig. 11b), resulting in a broader positive vertical velocity maximum farther downwind and excessive deposition and condensation. In contrast, there was twice as much snow observed upstream of the Wasatch (0.4 g kg^{-1}) than simulated (Fig. 14b), which suggests that the underprediction of snow aloft in the model was compensated by having too much cloud water aloft. At 3130 and 2812 m (Figs. 13c,d), the model also produced 2–3 times more cloud water than observed upstream of the Wasatch, while the model underpredicted the snow at these levels by about 50% (Figs. 14c,d). The model produced excessive cloud water upstream of the Wasatch even though the simulated vertical velocities were weaker than observed (cf. Fig. 11).

The size distributions of ice from the NOAA P-3 averaged for three flight legs are compared with the model (Fig. 15). At 4356 m MSL (Fig. 15a), the observed distribution is nearly exponential for sizes greater than 1 mm. The model had a similar size distribution, but it underpredicted the number of smaller crystals less than 2 mm. At 3756 m (Fig. 15b), the observed snow size distribution was not exponential, since there was a dramatic broadening of the observed ice spectra, with many aggregated particles greater than 6 mm. Most of these larger particles were observed over the blocked flow region, which was quantified by excluding that portion of the P-3 data between the crest and 30 km to the west of the barrier (Fig. 15b). When this region was excluded, the distribution was also closer to exponential. Meanwhile, the model at 3756 m dramatically underpredicted the concentration of larger snow crystals. The model also underpredicted the snow at 2812 (Fig. 15c) and 3130 m (not shown), where the observed snow distribution is still very broad, but it is more exponential than at 3756 m.

b. Microphysical budget

Figure 16 shows the dominant microphysical processes averaged horizontally and vertically within solid boxed region of Fig. 1b between 1900 and 2000 UTC in the 1.33-km run. Each process was normalized by the water vapor loss (WVL) rate within the volume, with process values greater than 5% of the WVL rate high-

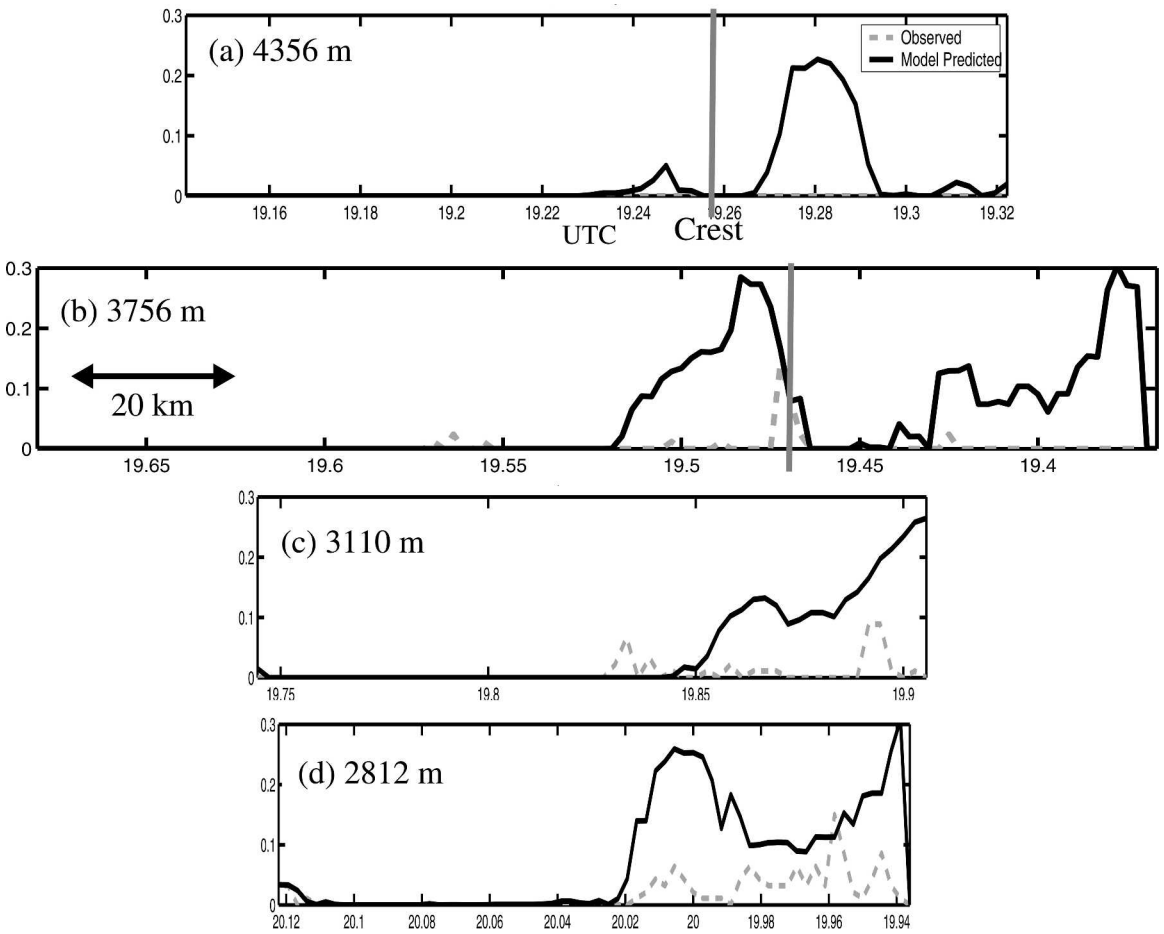

FIG. 13. Flight-level time series of liquid water mixing ratio (g kg^{-3}) from the King probe (dashed) and 1.33-km MM5 (solid) at (a) 4356, (b) 3756, (c) 3110, and (d) 2812 m MSL. The location of the crest is shown by the gray vertical line.

lighted in bold. The pathway to cloud water via condensation is the largest sink of water vapor over the windward slope (cond = 71% of WVL). Snow and cloud ice deposition (sdep and idep) accounts for most of the remainder of the WVL (29%). The cloud water leads to accretion by rain (racw = 5%), but there is little cloud water autoconversion (ccnr $\ll$ 1%). Accretion by rain accounts for about 20% of the rain fallout upstream of the crest, with the fallout scaling as 27% of WVL. Snowmelt accounts for over half of the rain generation and fallout upstream of the Wasatch; however, a relatively large fraction (30%) of snow produced is converted to graupel (scng = 7% of WVL). This graupel grows via riming (ggacw + gsacw = 16% of WVL), falls out (8% of WVL), or melts to account for about 35% of the rain growth (gmlt = 10% of WVL).

The precipitation efficiency (PE) is defined as the total amount of fallout of hydrometeors within a specified region divided by the total WVL within this same volume. The PE can be obtained by adding the fallout terms in the microphysical budget (rpsc, sprc, and gprc in Fig. 16), since the fallout is normalized by the WVL. The PE for the control run is 47%. Most of the condensate is lost by cloud water evaporation into the immediate lee of the crest (evap = 36%), while the remainder is lost to horizontal advection of snow and graupel (hadv_s = 5%; hadv_g = 1%). The simulated PE for this case is lower than that recently diagnosed for the Sierras (PE = 80%) using MM5 (Colle and Zeng 2004a), but similar to a strong cross-barrier flow event during the IMPROVE-2 field experiment (PE = 50%) over the Cascades (Colle et al. 2005). The Cascades are much wider than the Wasatch, which favors a larger PE, but the IMPROVE-2 PE was reduced by the significant snow spillover into the lee with the strong (>30 m s^{-1}) cross-barrier flow. Meanwhile, the relatively low PE for IPEX was the result of modest cross-barrier flow over the narrow Wasatch.

Overall, there was little cloud water and riming observed during this IPEX IOP event even though the

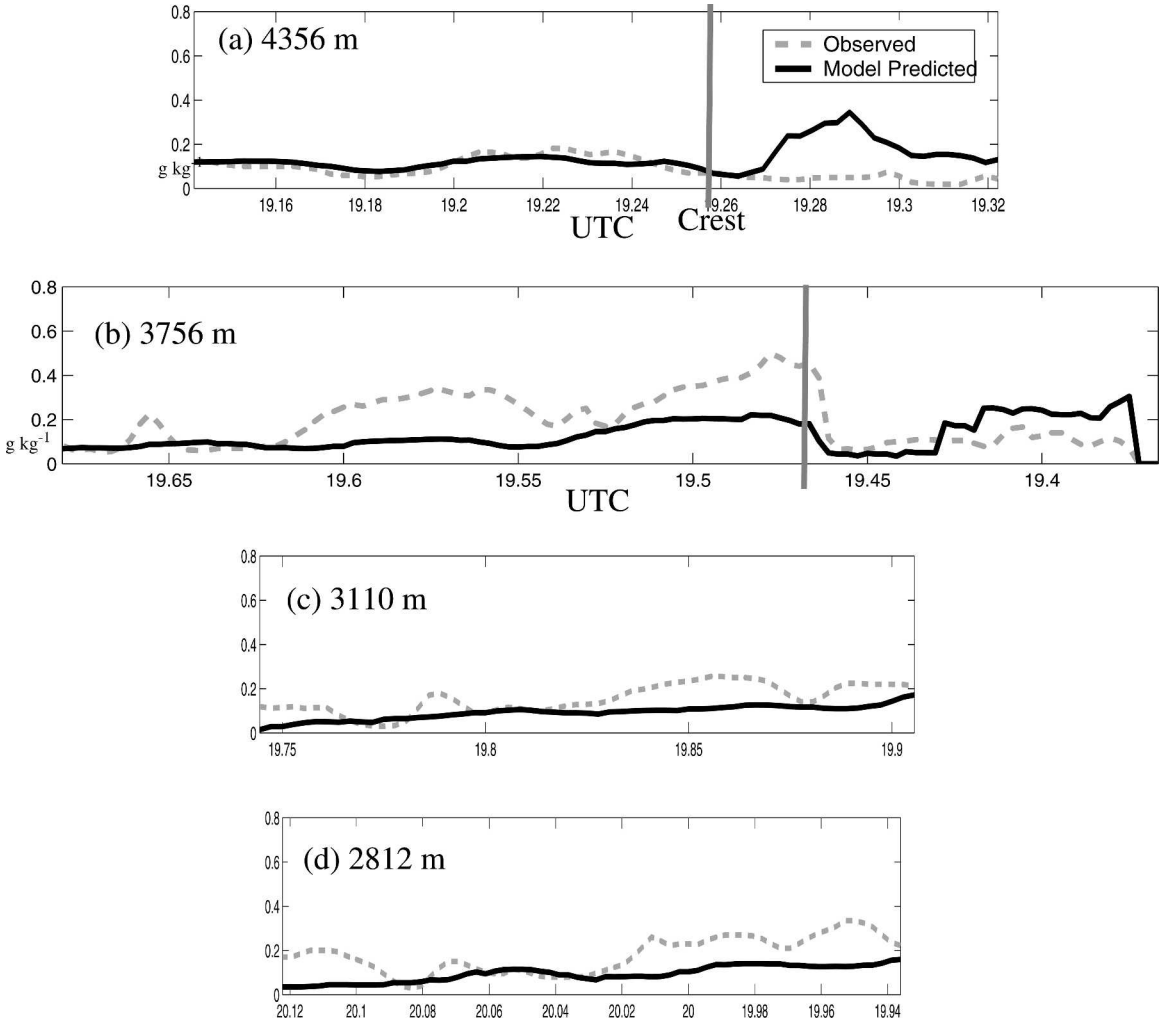

FIG. 14. Flight-level time series of snow mixing ratio (g kg^{-1}) derived from the composite 2DGC–2DP particle size spectra (gray dashed) and 1.33-km MM5 (black) at (a) 4356, (b) 3756, (c) 3110, and (d) 2812 m MSL. The location of the crest is shown by the gray vertical line.

vertical motions were comparable or stronger than in the MM5 (Figs. 11, 13). The MM5 tended to produce too much cloud water, which was compensated by having too little snow aloft. As a result, the relatively accurate surface precipitation amounts in the 1.33-km MM5 were obtained in spite of the likelihood that hydrometeor characteristics were poorly simulated.

c. Comparisons with 13–14 December 2001 of IMPROVE-2 and microphysical sensitivities

The microphysical verification results from IPEX IOP3 can be compared with some recent findings from IMPROVE-2 over the Oregon Cascades in December 2001 (Stoelinga et al. 2003). In particular, the 13–14 December IMPROVE-2 results described in Garvert et al. (2005a,b) and Colle et al. (2005) can be compared with the more narrow and continental Wasatch Front in IPEX. Table 1 highlights some of the important kinematic, thermodynamic, and microphysical differences between the two cases. Unlike IMPROVE-2, there was little cloud water and riming observed aloft during IPEX IOP3. There was more snow aloft in IPEX than IMPROVE-2, even though the cloud top in IPEX was about 1 km shallower than IMPROVE-2 (6–7 km versus 7–8 km). Previous studies have also shown that orographic clouds involving fronts over northern Utah primarily contain ice/snow and not much supercooled water (Sassen et al. 1990). Continental areas tend to have greater cloud condensation nuclei (CCN) concentrations than maritime regions (Marwitz 1987b); therefore, the lack of supercooled water over the Intermountain

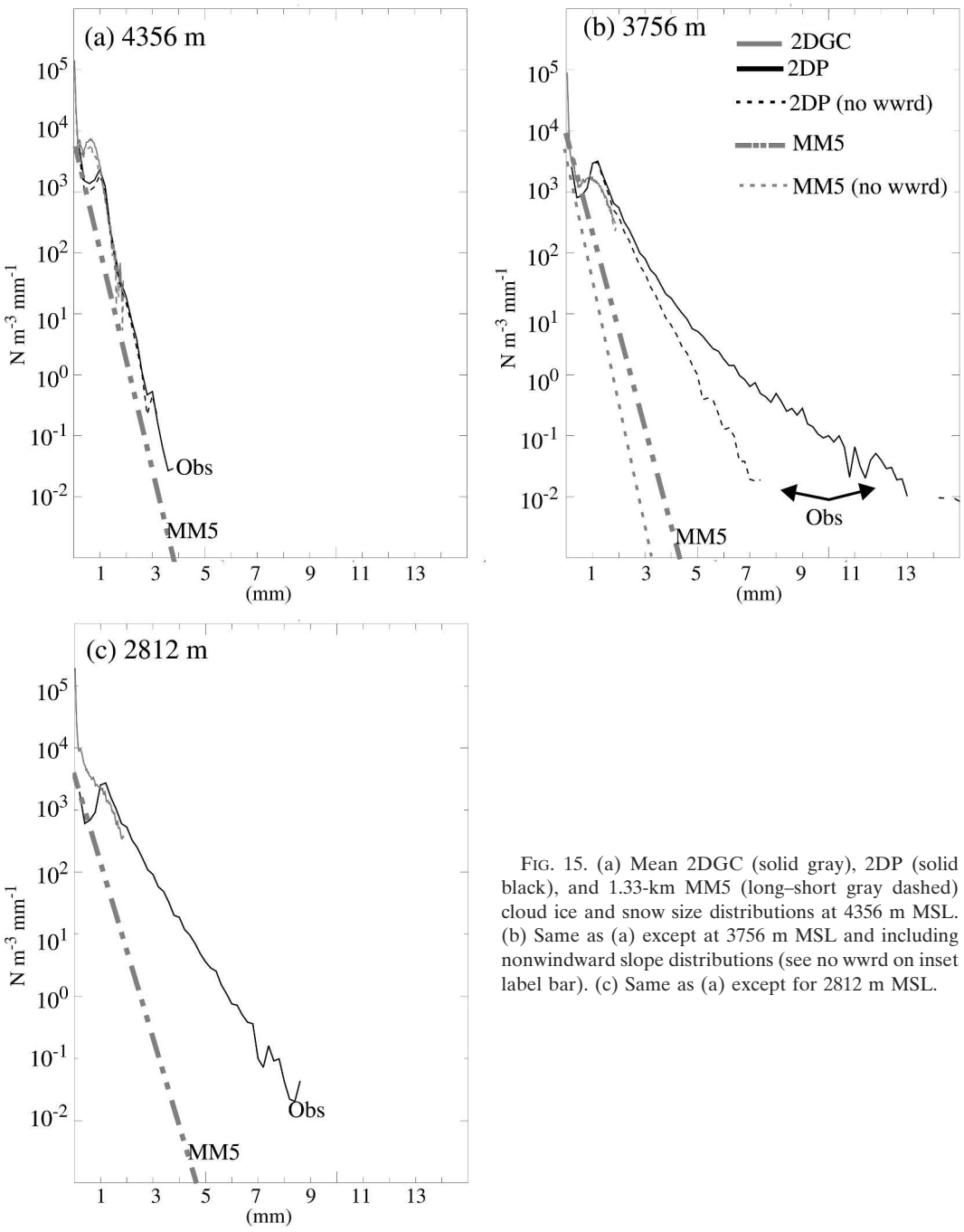

FIG. 15. (a) Mean 2DGC (solid gray), 2DP (solid black), and 1.33-km MM5 (long–short gray dashed) cloud ice and snow size distributions at 4356 m MSL. (b) Same as (a) except at 3756 m MSL and including nonwindward slope distributions (see no wwrd on inset label bar). (c) Same as (a) except for 2812 m MSL.

West has been attributed to the large number of smaller cloud droplets, which compete for available supersaturated water.

The CCN concentrations were not measured directly in either IMPROVE or IPEX, but the cloud droplet concentrations were obtained by a Forward Scattering Spectrometer Probe (FSSP) on the P-3 and Convair aircraft. Over the Wasatch during IPEX IOP3 the cloud water concentrations at −11°C (3700 m) were 100–300 cm^{-3} (not shown), while over the windward Cascades during 13–14 December 2001 of IMPROVE-2 the cloud droplet concentrations were 20–80 cm^{-3} at this temperature. Since there was 0.1–0.2 g kg^{-1} more cloud water mass observed during IMPROVE-2 at this temperature, this suggests that IMPROVE cloud droplet spectra are fewer in number but larger in size than IPEX.

The kinematic flow, moisture profile, and stability

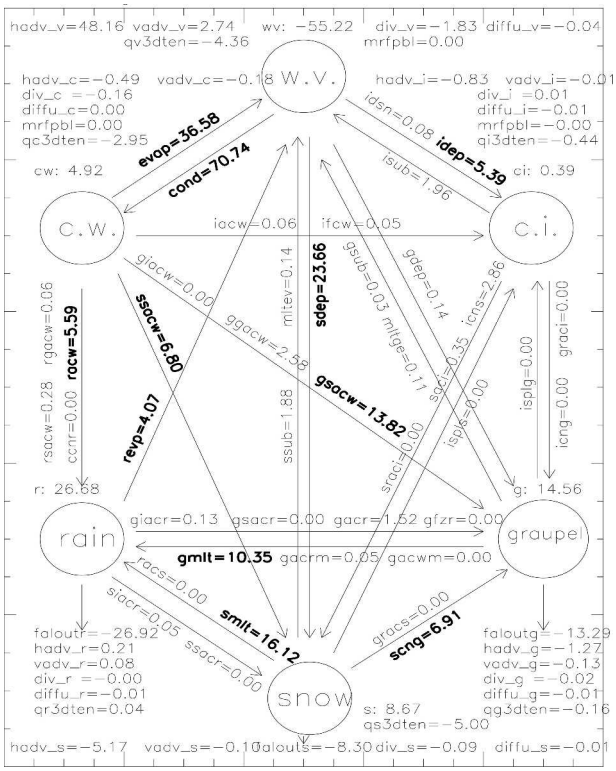

FIG. 16. Flowchart of the microphysical processes between 6 and 12 h of the control run for the box in Fig. 1b. The values shown are the ratio of each microphysical process rate to the total WVL rate (cond + sdep + gdep + idsn + idep) within the box. The processes are listed in the appendix. The sum of all the microphysical process tendencies for each species is given by (wv:, cw:, r, ci:, g:, and s:). This sum does not include horizontal advection and diffusion/divergence, which are labeled as hadv and other, respectively. The fallout tendency of rain (rprc), snow (sprc), graupel (gprc), and cloud ice (iprc) are also shown. Microphysical processes greater than 5% of the WVL rate are in bold.

were well simulated in both regions; however, during 13–14 December of IMPROVE-2 there was widespread overprediction of precipitation over the windward slopes and immediate lee of the crest. This overprediction was related to having too much snow production aloft. In contrast, there was little model overprediction of surface precipitation around the central Wasatch during IPEX IOP3, with the model within 20% of the observed at many locations (cf. Fig. 10). As in IMPROVE-2, the Reisner2 BMP produced too much supercooled water over the windward slope during IPEX (cf. Fig. 13). However, the cloud water overprediction for IMPROVE-2 was limited to the lower windward slope, and it transitioned to an underprediction over the crest as snow particles grew at the expense of the cloud water. Since the time scale for snow to advect across the Wasatch is much shorter than the Cascades, there was little impact of the excessive cloud water on

TABLE 1. A comparison of parameters and verification from the 13–14 Dec IMPROVE-2 IOP7 (13–14 Dec 2001) and the 12 Feb 2000 IPEX IOP.

Expt	Barrier half-width and average height above valley floor	Froude number and cross-barrier flow at crest level	Flow blocking	Cloud top (MSL)	0° and −15°C heights (ASL)	Surface precipitation errors	Cloud water errors	Snow errors
IMPROVE-2 IOP7	Cascades: 50 km; 2000 m	1.0–2.0 17 m s^{-1}	Partial	7–8 km	2.25 km and 4.50 km	50%–100% overprediction in lee and steep windward slopes	Over lower windward slope (2–3 km ASL): simulated (0.4–0.5 g kg^{-3}), observed (0.2–0.3 g kg^{-3})	Over windward slope (5–6 km ASL): simulated (0.35–0.55 g kg^{-3}), observed (0.10–0.25 g kg^{-3})
IPEX IOP3	Wasatch: 5 km; 1500 m	<1.0 below midmountain >1.5 above midmountain 10 m s^{-1}	Blocked below midmountain	6–7 km	1.75 km and 4.1 km	Within 25% over Wasatch; 25%–50% underprediction >20 km upstream of barrier	Over Wasatch (3–4 km ASL): simulated (0.1–0.25 g kg^{-3}), observed (0–0.1 g kg^{-3})	Over Wasatch (3–4 km ASL): simulated (0.2–0.3 g kg^{-3}), observed (0.4–0.55 g kg^{-3})

the snow in IPEX. Rather, the lack of snow in IPEX may have been compensated in the model by too much cloud water accretion, riming, and graupel production given the microphysical budget (Fig. 16), thus resulting in relatively accurate surface precipitation forecasts in spite of the likelihood that the snow distributions were poorly simulated aloft. Interestingly, over the southern Wasatch, which are much wider and more similar to the Cascades, the model overpredicted surface precipitation, consistent with that of IMPROVE-2. This suggests that wider barriers may be more sensitive to errors in microphysical details aloft, which is consistent with the larger snow sensitivities noted for wider barriers in Colle and Zeng (2004b).

Recent studies such as Colle et al. (2005), Colle and Zeng (2004a,b), and Thompson et al. (2004) have investigated parameters involving the intercept for the snow size distribution (Nos), snowfall speed, cloud water autoconversion, snow to graupel autoconversion, and CCN. For this IPEX study, the same sensitivity experiments were run as those in Colle et al. (2005) for 13–14 December of IMPROVE-2. For IPEX, it was found that changing the cloud to rain autoconversion from Berry and Reinhardt (1974) to Kessler (1969), or implementing a slower snow aggregate fall speed for snow (Cox 1988), had little impact on the results (not shown). This is consistent with the small amount of autoconversion in the control run (cf. Fig. 16) and the limited snow aloft in the model.

Colle et al. (2005) showed that using a different intercept for the snow size distribution can produce relatively large differences in snow and cloud water aloft. The control Reisner2 uses a snow intercept parameter that depends on temperature (NosT) (Thompson et al. 2004). As compared to a fixed Nos = 2×10^7 m^{-4} in other well-known BMPs (Lin et al. 1983; Rutledge and Hobbs 1983), NosT decreases as the temperature increases, which results in more larger snow particles at lower altitudes and fewer smaller particles higher aloft. When Nos is a function of snow mixing ratio (Nosqs) (Reisner et al. 1998), it favors even more large snow particles and fewer small particles than the other Nos approaches (Colle and Zeng 2004a). For IMPROVE-2, a Nosqs slightly reduced the snow aloft, but snow overprediction was still prevalent. A simulation using Nosqs during IPEX also produced 0.05 g kg^{-1} more snow and 0.1–0.2 g kg^{-1} more supercooled water aloft (not shown), but this worsens, rather than improves the forecast in the CTL (cf. Fig. 12).

A fixed Nos in IMPROVE-2 enhanced the snow overprediction and cloud water underprediction over the Cascade crest and resulted in spurious bull's-eyes of surface precipitation in the immediate lee of the barrier. A simulation using a fixed Nos for IPEX was completed, which yielded more positive results (Fig. 17). As compared to the CTL for the cross section averaged between 1900 and 2000 UTC 12 February (Fig. 12), the fixed Nos nearly doubles the amount of snow aloft from 0.35 to 0.65 g kg^{-1}, and it reduces the amount of graupel and supercooled water by a factor of 2. As a result, as compared to the NOAA P-3 flight legs (bold numbers in Fig. 17a), the snow underprediction is less than 0.1 g kg^{-1} over the Wasatch, and the cloud water is within 0.05 g kg^{-1} of the observed. The fixed Nos only increased the 6-h surface precipitation over the central Wasatch and slightly upstream by 1–3 mm (5%–10%) (not shown), which actually improved the verification slightly. These fixed Nos simulations suggest that there were many more smaller ice particles in the observations that grew at the expense of the cloud water as compared to the CTL and Nosqs runs.

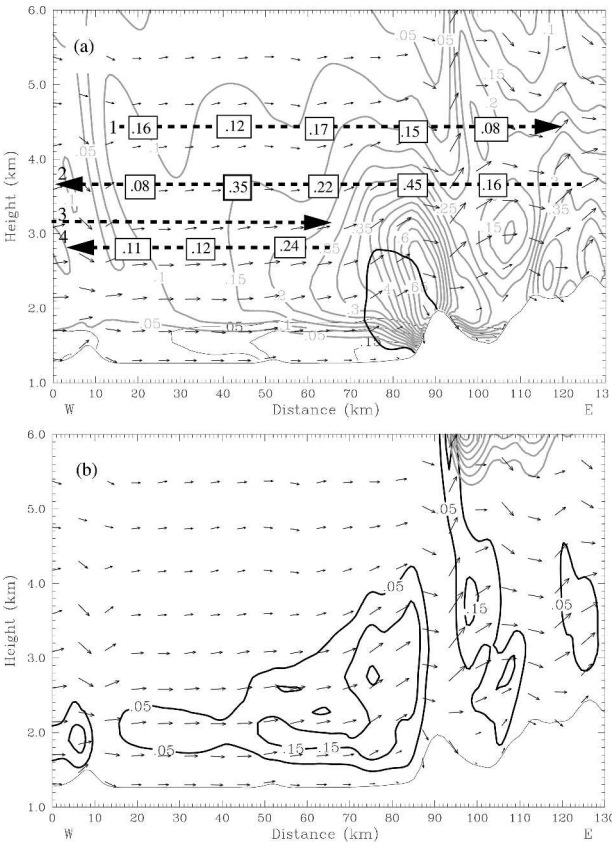

FIG. 17. Cross section for the fixed Nos experiment along BC averaged between 1900 and 2000 UTC 12 Feb showing snow (gray) and graupel (bold black) every 0.05 g kg^{-1}, rain (thin black below 2 km) every 0.10 g kg^{-1}, and circulation vectors in the cross section. The NOAA P-3 legs are shown by the dashed lines 1–4, with select observed snow mixing ratios (g kg^{-1}) in the boxes. (b) Same simulation as (a) except for cloud water (solid) every 0.10 g kg^{-1} and cloud ice (gray) every 0.02 g kg^{-1}.

The initial generation of graupel in Reisner2 is determined primarily by the snow to graupel autoconversion (scng), and this process is initiated when the amount of snow riming (psacw) exceeds depositional growth (sdep) by a factor of 2.5 (Thompson et al. 2004). An experiment was completed in which this factor was reduced to 1.0, a threshold that was applied in earlier versions of Reisner2 (Reisner et al. 1998). This change helped for IMPROVE-2, since it reduces the amount of snow aloft that can spill over the crest (Colle et al. 2005); however, the same approach used for IPEX worsened the microphysical verification aloft, with a 0.05 g kg^{-1} decrease in snow at flight level and a 0.1–0.2 g kg^{-1} increase in cloud water (not shown).

Another issue in the BMPs is the sensitivity to the aerosol/CCN concentrations. CCN is not used directly in the Reisner2 BMP, but there is a parameter that sets the cloud droplet concentrations (CNP), which determines the amount of cloud to rain autoconversion (Thompson et al. 2004). Currently, the CNP parameter is specified as 100 cm^{-3}, but this value was increased to 600 cm^{-3} to represent a larger continental droplet number distribution. However, this change in the IPEX simulation was found to have little impact on the snow field, and the cloud water nearly doubled to a maximum of 0.6 g kg^{-3} over the windward slope around 3 km MSL (not shown). In the Reisner2 BMP, increasing the CNP results in less autoconversion and thus greater amounts of cloud water. Unfortunately, this leads to greater cloud water overprediction over the windward slope and spurious supercooled rain autoconversion upward to 3 km MSL. Future efforts of this BMP will need to treat CCN impacts more directly between the continental and maritime regions.

In summary, the largest benefit was seen using a fixed intercept for the snow size distribution (Nos); however, a fixed Nos has been considered problematic in other geographic locations (Reisner et al. 1998; Colle et al. 2005). The fact that this simple Nos approach improved the IPEX forecast suggests that more work is needed with this parameter, perhaps relating it cloud-top height, vertical motion, or crystal type.

5. Processes influencing the windward kinematic structure and precipitation distribution

Although the model has clear deficiencies in the microphysics aloft, it realistically simulated many of the observed kinematic and precipitation structures over the Wasatch. As a result, this section highlights a few more sensitivity studies to quantify the important factors that led to the upstream-observed flow and precipitation transitions.

a. Upstream terrain and lake effects

The observed and simulated flow structures during IPEX IOP3 are similar to the Neiman et al. (2002) conceptual model along the California coast, with shallow upstream flow blocking enhancing the low-level convergence and precipitation upstream of the barrier. However, unlike the West Coast, the Wasatch has significant terrain upstream to the southwest of the Wasatch. Cox et al. (2005) hypothesized that the GSL and topography to the south of the lake may have influenced the position and strength of the windward convergence zone during IOP3. In particular, the reduced surface drag over the GSL favors more geostrophic southwesterly flow over the lake, which converges with the weaker and more ageostrophic flow immediately downwind of the lake. Cox et al. (2005) also noted that the flow channeling between the Oquirrh and Stansbury Mountains to the south of the lake may favor southerly ageostrophic flow extending farther upstream of the Wasatch than if the upstream flow was unperturbed to the south.

To quantify the impact of upstream terrain and the GSL on the flow and precipitation structures, a series of MM5 sensitivity experiments were completed by systematically removing certain terrain features. The Global Data Assimilation System (GDAS) pressure-level analyses were used to obtain data for areas below the removed terrain, since GDAS cannot resolve these small-scale terrain features. First, a simulation was completed in which the terrain to the south of the lake was removed and replaced by flat land (NOTER run). Without the ridges to the south and their associated downslope warming, the surface temperatures were 1°–2°C cooler over the southern GSL and adjacent to the Wasatch than in the CTL by 1800 UTC 12 February (Figs. 18a,b). The cooler temperatures and enhanced pressure gradient adjacent to the Wasatch results in 2–3 m s^{-1} stronger flow in the NOTER run, but the location of the upstream convergence zone to the east of the GSL in the NOTER is similar to the control. The upstream flow convergence was 20%–30% stronger in the NOTER immediately west of OGD (not shown), resulting in a somewhat greater precipitation enhancement in the NOTER adjacent to the Wasatch. The largest kinematic differences with the NOTER are immediately to the north of the Oquirrh Mountains, where the absence of flow splitting results in only weak convergence in the NOTER run. The cooler temperatures adjacent to the Wasatch did slow the eastward advance of the windward convergence boundary in the NOTER run by a few hours after 1800 UTC (not shown). Overall, even without the terrain to the south, significant

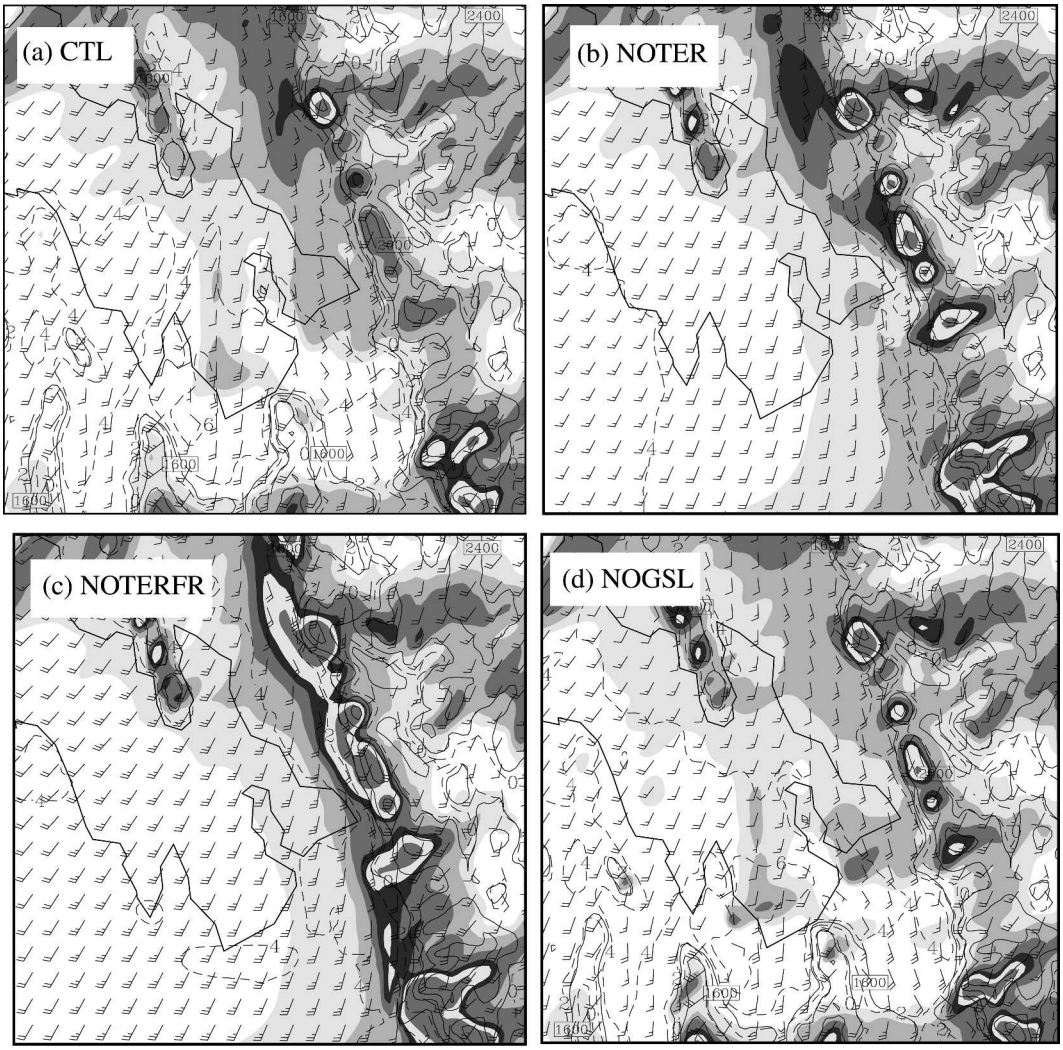

FIG. 18. Surface winds (full barb = 10 kt), temperature (dashed every 2°C), and model reflectivities (shaded using scale in Fig. 5a) for the (a) CTL, (b) NOTER, (c) NOTERFR, and (d) NOGSL experiments at 1800 UTC 12 Feb (hour 6).

blocking and upstream enhancement of the precipitation occurred.

It is interesting that the upstream scale of the ageostrophic southerlies for the NOTER run extends farther west of the Wasatch near the southeast corner of the GSL than the northeast corner of the lake (Fig. 18a). This suggests that the reduced friction over the GSL may allow the greater southwesterly momentum to extend farther eastward than to the south of the lake. To test this hypothesis, a simulation was completed in which the flat land to the south was replaced by water at the same temperature of the GSL (NOTERFR run). As a result, this simulation is analogous to the situation along the West Coast, in which flow over water encounters an elongated coastal barrier. With the larger area of upstream water in the NOTERFR run (Fig. 18c), the surface winds are 3 m s^{-1} stronger and slightly more southwesterly than the NOTER simulation. As a result of the stronger ambient southwesterlies in the NOTERFR run, the upstream scale of the blocked flow is reduced by 5–10 km as compared to the CTL and NOTER, especially to the southeast of the GSL. However, the flow is still blocked by the Wasatch in the NOTERFR run. The combination of stronger upstream southwesterlies and the nearly terrain-parallel flow results in stronger low-level convergence and more intense precipitation 5–10 km upstream of the Wasatch than the control simulation.

The calculated Rossby radius, $N_m h_m/f$, for the NOTERFR is about 75 km (moist $N_m = 0.005$ s^{-1}; $h_m = 1500$ m; $f = 10^{-4}$ s^{-1}), while the observations indicate upstream blocking on the order of 25–50 km in the control

and 10–20 km in the NOTERFR run. This suggests that upstream terrain and land surface properties may have a profound impact on the intensity and upstream scale of the flow blocking as compared to scale analysis (Overland and Bond 1995). To further isolate the impact of the GSL on the flow blocking and precipitation structures, the lake was replaced with a flat land surface and a ground temperature similar to that just west of the lake (NOGSL run). With the increased surface friction over the Lake in the NOGSL run the flow was 2–3 m s^{-1} weaker over the lake than the control (Fig. 18d). The transition to south-southwesterly flow also extended 5–10 km farther west in the NOGSL run. The low-level convergence was 30%–40% weaker in the NOGSL than the control (not shown), which resulted in weaker precipitation enhancement west of the Wasatch in the NOGSL. This result in consistent with the hypothesis in Cox et al. (2005), in which the differential surface drag to the east of the lake enhanced the wind transitions and low-level convergence to the east of the lake. Therefore, the GSL is an important factor in modulating the flow-blocking response adjacent to the central Wasatch.

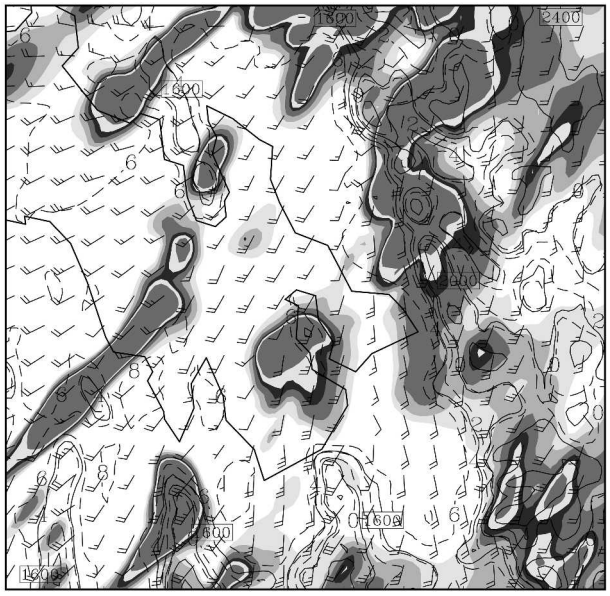

FIG. 19. Surface winds (full barb = 10 kt), temperature (dashed every 2°C), and model reflectivities (shaded using scale in Fig. 5a) for the NOEVMLT experiment at 1800 UTC 12 Feb (hour 6).

b. Diabatic cooling effects

Numerous studies have shown that diabatic effects can modulate the strength of the terrain flow blocking. For example, Marwitz (1987a) showed that melting effects over the windward Sierra Nevada increased the low-level stratification, which favored increased flow blocking and an increased barrier jet. Colle et al. (2002) also showed that the low-level flow blocking upstream of the California coastal range was enhanced by low-level diabatic cooling by precipitation. During IPEX IOP3 there was no low-level advective source of cold air to the south of the Wasatch; therefore, low-level diabatic effects may have been important in maintaining enough stratification to promote blocking.

A separate IPEX simulation was completed in which the diabatic cooling effects from evaporation and melting were turned off (NOEVMLT) in all domains. By 1800 UTC 12 February (Fig. 19), there was southwesterly surface flow to the east of the GSL in the NOEVMLT run, with little or no flow blocking evident adjacent to the central Wasatch. Without the low-level diabatic cooling effects from falling precipitation, the surface temperatures were 2°–3°C warmer than the CTL (Fig. 18a). The warmer boundary layer decreased the stability to slightly more unstable than moist neutral below 700 mb (not shown), and this conditional instability eliminated the potential for flow blocking and several areas of convective precipitation developed across the domain. These results suggest that diabatic cooling from precipitation during IOP3 was important in maintaining enough stability to favor flow blocking. There is some potential for some positive feedback, since the flow blocking results in enhanced precipitation extending 25–50 km upstream of the barrier. This precipitation leads to additional diabatic cooling and increased stratification at low levels. In fact, it was observed that during IPEX IOP3 the near-surface stability increased as the rain rates increased between 1800 and 2100 UTC 12 February (Figs. 2c,d). However, flow blocking did not increase with time since this stability increase was offset by the stronger cross-barrier flow near crest level.

6. Summary and conclusions

This study investigates the 12 February 2000 IPEX IOP3 event using high-resolution MM5 simulations down to 1.33-km grid spacing. This modeling effort builds on the observational analysis of SSC and Cox et al. (2005), in which the synoptic and mesoscale structural evolution of the case are discussed. The goals of this study were to 1) use the model to better understand the flow and precipitation structures around the Wasatch Mountains, 2) determine whether there were any flow impacts from upstream terrain, the GSL, and diabatic effects from precipitation, and 3) validate the model precipitation and microphysics aloft, such as that the microphysical errors can be compared with other locations and microphysical schemes.

The MM5 was verified using in situ aircraft data, radiosondes, ground-based radar, and surface observations. The model realistically simulated the low-level convergence 20–40 km upstream of the Wasatch Mountains, which developed as a result of partial flow blocking of the 8–12 m s^{-1} southwesterlies approaching the barrier. As observed, the model had rapid upward ascent associated with the leading edge of this flow blocking, which resulted in a sharp gradient in precipitation enhancement about 20 km upstream of the Wasatch. As noted in the Doppler velocities, the simulated blocked flow was shallow and limited to below midmountain level. Meanwhile, the crest-level flow resulted in strong mountain-wave-induced lee subsidence between 1 and 2 m s^{-1} that was well simulated; however, the MM5 at 1.33 km could not resolve the multiple lee waves to the east of the Wasatch. After the passage of a midlevel trough increased in barrier-normal flow, the model properly simulated the reduction in flow blocking and the resulting movement of the low-level convergence zone and precipitation enhancement toward the Wasatch; however, the model midlevel trough aloft and wind shift to westerly aloft were weaker than observed.

The model was verified against surface precipitation gauges across the Wasatch for the 1800 UTC 12 February to 0000 UTC 13 February period. The 1.33-km MM5 underpredicted the precipitation upstream of the Wasatch around the GSL, but the amounts were within 25% of the observed over the central Wasatch at all stations. There were substantial improvements in precipitation amount as the grid spacing is decreased from 12- to 4-km grid spacing, and only the 1.33-km domain resolved the narrow Wasatch peak. The large precipitation improvements from 12 to 4 km are consistent with longer-term precipitation verification results of Hart et al. (2004) over this region using the MM5.

Even though the surface precipitation amounts were relatively close to observed over the central Wasatch, the Reisner2 bulk microphysical scheme (BMP) produced too much supercooled cloud water aloft and too little snow as compared to in situ aircraft data. A model microphysical budget revealed that the Reisner2 obtained over half of the windward surface precipitation through riming and cloud water accretional processes rather than primarily depositional snow growth and aggregation. This compensation of cloud water accretion led to a reasonable surface precipitation forecast for IPEX IOP3, but it may not for other cases. Furthermore, having accurate microphysical quantities aloft in the model is important for other applications, such as the forecast of aircraft icing.

A few BMP simulations were also completed using different intercepts for the snow size distribution, riming rates, and cloud condensation nuclei amounts. A snow intercept that allows for greater snow concentrations at colder temperatures helps improve the snow predictions aloft and reduce the cloud water overprediction for this particular event. Increasing the cloud droplet concentrations to more continental values (600 cm^{-3}) resulted in more cloud water overprediction.

The microphysical verification results can be compared with the 13–14 December 2001 IMPROVE-2 event over the Oregon Cascades (Garvert et al. 2005b). Both IPEX and IMPROVE overpredicted cloud water when the ambient flow encountered the first windward ridge, which is the Wasatch barrier itself for IPEX, so this appears to be a robust problem in the Reisner2 scheme. However, for IMPROVE-2 this cloud water overprediction transitioned to underprediction over the crest as a result of excessive snow growth aloft. In contrast, there was underprediction of snow aloft in IPEX and the model had too much riming with the abundant supercooled water. Additional investigation is needed to determine the reasons for the dramatic differences in snow growth aloft between the two areas, and more field cases need to be analyzed to determine the generality of the IMPROVE and IPEX results.

Several sensitivity runs determined what impact the GSL and the series of basin and range topography to the south of the lake may have had on the flow and temperatures downstream toward the Wasatch. Without the downslope warming from the ridges to the south of the lake, the surface temperatures were 1°–2°C cooler, which favored an enhanced pressure gradient adjacent to the Wasatch and 2–3 m s^{-1} stronger low-level flow. The upstream flow convergence was 20%–30% stronger immediately west of the Wasatch, resulting in a somewhat greater precipitation enhancement than the control. When the flat land to the south of the lake was changed to water, which is analogous to the situation along the West Coast, the surface winds were 3 m s^{-1} stronger and slightly more southwesterly. As a result, the upstream scale of the blocked flow is reduced by 5–10 km as compared to the control, especially to the southeast of the GSL. The combination of stronger upstream southwesterlies and the nearly terrain-parallel flow results in stronger low-level convergence and more intense precipitation 5–10 km upstream of the Wasatch than the control simulation. Finally, when the GSL was replaced by flat land, the low-level convergence and precipitation enhancement within the flow-blocking region was reduced.

Although the observations and simulation showed

little evidence of a well-defined stable layer near the surface induced by diabatic cooling, an experiment without diabatic cooling produced boundary layer temperatures that were 3°–4°C warmer than the control. As a result, the sounding was more unstable and resulted in convective development around the Wasatch and limited flow blocking. Therefore, diabatic effects from precipitation can play a major role in modulating the flow blocking as compared to dry dynamics.

Acknowledgments. This research was supported by National Science Foundation Grants ATM-0094524 and ATM-0085318. Comments and suggestions by Matt Garvert and three anonymous reviewers helped to improve the manuscript. We thank Tom Wilson and Dr. Mark Stoelinga at the University of Washington for providing the processed Forward Scattering Spectrometer Probe (FSSP) data from IMPROVE-2. We also thank all the individuals and organizations who participated in the planning and execution of IPEX. Thanks also to the staff of the NOAA Aircraft Operations Center for their efforts in collecting airborne observations. Use of the MM5 was made possible by the Microscale and Mesoscale Meteorological (MMM) Division of the National Center for Atmospheric Research (NCAR), which is supported by the National Science Foundation.

APPENDIX

Abbreviation and Description of Each Microphysical Process in the Reisner2 Scheme

1	Psaci	Accretion of cloud water by snow
2	Pracw	Accretion of cloud water by rainwater
3	Pccnr	Autoconversion of cloud water by rainwater
4	Psraci, Pgraci	Collection of cloud ice by rain
5	Pggacw, Prgacw	Collection of cloud water by graupel
6	Pssacw, Pgsacw, Prsacw	Collection of cloud water by snow
7	Pgacr	Collection of rain by graupel
8	Pssacr, Pgsacr	Collection of rain by snow
9	Pracs, Pgracs	Collection of snow by rain
10	Cond, evap	Condensation/evaporation
11	Pscng	Conversion from snow to graupel
12	Picng	Conversion from cloud ice to graupel
13	Picns	Conversion from cloud ice to snow
14	Pidep, Pisub	Deposition/sublimation of cloud ice
15	Pgdep, Pgsub	Deposition/sublimation of graupel
16	Psdep, Pssub	Deposition/sublimation of snow
17	Pgacwm	Enhanced melting of graupel by collection of cloud water
18	Pgacrm	Enhanced melting of graupel by collection of rainwater
19	Pmltge	Evaporation of melting graupel
20	Pmltev	Evaporation of melting snow
21	Prevp	Evaporation of rainwater
22	Pifzc, Pihfz	Hetero/homogeneous freezing of cloud droplets
23	Psiacr, Pgiacr	Freezing of rain by collision with ice
24	Pgfr	Freezing of rain to graupel
25	Pispls, Pisplg	Ice multiplication process
26	Pidsn	Initiation (nucleation) of cloud ice
27	Pgmlt	Melting of graupel
28	Psmlt	Melting of snow
29	Pimlt	Melting of cloud ice
30	Piiacw, Pgiacw	Riming of cloud ice

REFERENCES

Baumgardner, D., and A. Korolev, 1997: Airspeed corrections for optical array probe sample volumes. *J. Atmos. Oceanic Technol.,* **14,** 1224–1229.

Berry, E. X., and R. L. Reinhardt, 1974: An analysis of cloud drop growth by collection. Part IV: A new parameterization. *J. Atmos. Sci.,* **31,** 2127–2135.

Bougeault, P., and Coauthors, 2001: The MAP Special Observing Period. *Bull. Amer. Meteor. Soc.,* **82,** 433–462.

Colle, B. A., 2004: Sensitivity of orographic precipitation to changing ambient conditions and terrain geometries: An idealized modeling perspective. *J. Atmos. Sci.,* **61,** 588–606.

——, and Y. Zeng, 2004a: Bulk microphysical sensitivities and pathways within the MM5 for orographic precipitation. Part I: The Sierra 1986 event. *Mon. Wea. Rev.,* **132,** 2780–2801.

——, and ——, 2004b: Bulk microphysical sensitivities and pathways within the MM5 for orographic precipitation. Part II: Impact of different bulk schemes, barrier width, and freezing level. *Mon. Wea. Rev.,* **132,** 2802–2815.

——, C. F. Mass, and K. J. Westrick, 2000: MM5 precipitation verification over the Pacific Northwest during the 1997–99 cool seasons. *Wea. Forecasting,* **15,** 730–744.

——, B. F. Small, and M.-J. Yang, 2002: Numerical simulations of a landfalling cold front observed during COAST: Rapid evolution and responsible mechanisms. *Mon. Wea. Rev.,* **130,** 1945–1966.

——, F. Garvert, J. B. Wolfe, C. F. Mass, and C. P. Woods, 2005: The 13–14 December 2001 IMPROVE-2 event. Part III: Simulated microphysical budgets and sensitivity studies.. *J. Atmos. Sci.,* **62,** 3535–3558.

Cox, G. P., 1988: Modeling precipitation in frontal rainbands. *Quart. J. Roy. Meteor. Soc.,* **114,** 115–127.

Cox, J. A., W. J. Steenburgh, D. E. Kingsmill, J. Shafer, B. A. Colle, O. Bousequet, B. F. Smull, and H. Cai, 2005: The kinematic structure of a Wasatch Mountain winter storm during IPEX IOP3. *Mon. Wea. Rev*., **133,** 521–542.

Fovell, R. G., and Y. Ogura, 1988: Numerical simulation of a midlatitude squall line in two dimensions. *J. Atmos. Sci.,* **45,** 3846–3879.

Garvert, M. F., B. A. Colle, and C. F. Mass, 2005a: The 13–14 December 2001 IMPROVE-2 event. Part I: Synoptic and mesoscale evolution and comparison with a mesoscale model simulation. *J. Atmos. Sci.,* **62,** 3474–3492.

——, C. P. Woods, B. A. Colle, C. F. Mass, P. V. Hobbs, M. P. Stoelinga, and J. B. Wolfe, 2005b: The 13–14 December 2001 IMPROVE-2 Event. Part II: Comparisons of MM5 model simulations of clouds and precipitation with observations. *J. Atmos. Sci.,* **62,** 3520–3534.

Gilmore, M. S., J. M. Straka, and E. N. Rasmussen, 2004: Precipitation and evolution sensitivity in simulated deep convective storms: Comparisons between liquid-only and simple ice and liquid phase microphysics. *Mon. Wea. Rev.,* **132,** 1897–1916.

Grell, G. A., J. Dudhia, and D. R. Stauffer, 1994: A description of the fifth-generation Penn State/NCAR Mesoscale Model (MM5). NCAR Tech. Note NCAR/TN-398+STR, 138 pp. [Available from National Center for Atmospheric Research, P. O. Box 3000, Boulder, CO 80307.]

Hart, K. A., W. J. Steenburgh, D. J. Onton, and A. J. Siffert, 2004: An evaluation of mesoscale-model-based model output statistics (MOS) during the 2002 Olympic and Paralympic Winter Games. *Wea. Forecasting,* **19,** 200–218.

Heymsfield, A. J., and J. L. Parrish, 1978: A computational technique for increasing the effective sampling volume of the PMS two-dimensional particle size spectrometer. *J. Appl. Meteor.,* **17,** 1566–1572.

——, and D. Baumgardner, 1985: Summary of a workshop on processing 2-D probedata. *Bull. Amer. Meteor. Soc.,* **66,** 437–440.

——, S. Lewis, A. Bansemer, J. Iaquinta, L. M. Miloshevich, M. Kajikawa, C. Twohy, and M. R. Poellot, 2002: A general approach for deriving the properties of cirrus and stratiform ice cloud particles. *J. Atmos. Sci.,* **59,** 3–29.

Hong, S.-Y., and H.-L. Pan, 1996: Nonlocal boundary layer vertical diffusion in a medium-range forecast model. *Mon. Wea. Rev.,* **124,** 2322–2339.

Houze, R. A., Jr., and S. Medina, 2005: Turbulence as a mechanism for orographic precipitation enhancement. *J. Atmos. Sci.,* **62,** 3599–3623.

Jiang, Q., 2003: Moist dynamics and orographic precipitation. *Tellus,* **55A,** 301–316.

Jorgensen, D. P., 1984: Mesoscale and convective-scale characteristics of mature hurricanes. Part I: General observations by research aircraft. *J. Atmos. Sci.,* **41,** 1268–1286.

——, and M. A. LeMone, 1989: Vertically velocity characteristics of oceanic convection. *J. Atmos. Sci.,* **46,** 621–640.

Kessler, E., 1969: *On the Distribution and Continuity of Water Substance in Atmospheric Circulations. Meteor. Monogr.,* No. 32, Amer. Meteor. Soc., 84 pp.

King, W. D., D. A. Parkin, and R. J. Handsworth, 1978: A hot-wire liquid water device having fully calculable response characteristics. *J. Appl. Meteor.,* **17,** 1809–1813.

Klemp, J. B., and D. R. Durran, 1983: An upper boundary condition permitting internal gravity wave radiation in numerical mesoscale models. *Mon. Wea. Rev.,* **111,** 430–444.

Knollenberg, R. G., 1970: The optical array: An alternative to scattering or extinction for airborne particle size determination. *J. Appl. Meteor.,* **9,** 86–103.

Korolev, A. V., and J. W. Strapp, 2002: Accuracy of measurements of cloud ice water content by the Nevzorov probe ice. *Proc. 40th Aerospace Sciences Meeting & Exhibit,* AIAA 2002-0679, Reno, NV, American Institute of Aeronautics and Astronautics. [Available online at http://www.airs-icing.org/publications/publications.htm.]

——, ——, and G. A. Isaac, 1998a: Evaluation of the accuracy of PMS optical array probes. *J. Atmos. Oceanic Technol.,* **15,** 708–720.

——, ——, ——, and A. N. Nevzorov, 1998b: The Nevzorov airborne hotwire LWC-TWC probe: Principle of operation and performance characteristics. *J. Atmos. Oceanic Technol.,* **15,** 1495–1510.

——, G. A. Isaac, and J. Hallett, 2000: Ice particle habits in stratiform clouds. *Quart. J. Roy. Meteor. Soc.,* **126,** 2873–2902.

Lin, Y. L., R. Farley, and H. D. Orville, 1983: Bulk parameterization of the snow field in a cloud model. *J. Climate Appl. Meteor.,* **22,** 1065–1092.

Locatelli, J. D., and P. V. Hobbs, 1974: Fallspeeds and masses of solid precipitation particles. *J. Geophys. Res.,* **79,** 2185–2197.

Marwitz, J. D., 1987a: Deep orographic storms over the Sierra Nevada. Part I: Thermodynamic and kinematic structure. *J. Atmos. Sci.,* **44,** 159–173.

——, 1987b: Deep orographic storms over the Sierra Navada. Part II: The precipitation processes. *J. Atmos. Sci.,* **44,** 174–185.

Mass, C. F., D. Ovens, K. W. Westrick, and B. A. Colle, 2002: Does increasing horizontal resolution produce better forecasts? The results of two years of real-time numerical weather prediction in the Pacific Northwest. *Bull. Amer. Meteor. Soc.,* **83,** 407–430.

McFarquhar, G. M., and R. A. Black, 2004: Observations of particle size and phase in tropical cyclones: Implications for mesoscale modeling of microphysical processes. *J. Atmos. Sci.,* **61,** 422–439.

Medina, S., and R. A. Houze Jr. 2003: Air motions and precipitation growth in Alpine storms. *Quart. J. Roy. Meteor. Soc.,* **129,** 345–371.

——, B. F. Smull, R. A. Houze Jr., and M. Steiner, 2005: Cross-barrier flow during orographic precipitation events: Results from MAP and IMPROVE. *J. Atmos. Sci.,* **62,** 3580–3598.

Neiman, P. J., F. M. Ralph, A. B. White, D. E. Kingsmill, and P. O. G. Persson, 2002: The statistical relationship between upslope flow and rainfall in California's coastal mountains: Observations during CALJET. *Mon. Wea. Rev.,* **130,** 1468–1492.

Overland, J. E., and N. A. Bond, 1995: Observations and scale analysis of coastal wind jets. *Mon. Wea. Rev.,* **123,** 2934–2941.

Ralph, F. M., and Coauthors, 1999: The California Land-Falling Jets Experiment (CALJET): Objectives and design of a coastal atmosphere–ocean observing system deployed during a strong El Nino. Preprints, *Third Symp. on Integrated Observing Systems,* Dallas, TX, Amer. Meteor. Soc., 78–81.

Reisner, J., R. M. Rasmussen, and R. T. Bruintjes, 1998: Explicit forecasting of supercooled liquid water in winter storm using the MM5 mesoscale model. *Quart. J. Roy. Meteor. Soc.,* **124,** 1071–1107.

Rutledge, S. A., and P. V. Hobbs, 1983: The mesoscale and microscale structure and organization of clouds and precipitation in mid-latitude cyclones: A model for the "seeder-feeder" process in warm-frontal rainbands. *J. Atmos. Sci.,* **40,** 1185–1206.

Sassen, K., A. W. Huggins, A. Long, J. B. Snider, and R. Meitin, 1990: Investigations of a winter mountain storm in Utah. Part II: Mesoscale structure, supercooled liquid water development, and precipitation processes. *J. Atmos. Sci.,* **47,** 1323–1350.

Schultz, D. M., and Coauthors, 2002: Understanding Utah winter storms: The Intermountain Precipitation Experiment. *Bull. Amer. Meteor. Soc.,* **83,** 189–210.

Stoelinga, M., and Coauthors, 2003: Improvement of microphysical parameterizations through observational verification experiments (IMPROVE). *Bull. Amer. Meteor. Soc.,* **84,** 1807–1826.

Thompson, G., R. M. Rasmussen, and K. Manning, 2004: Explicit forecasts of winter precipitation using an improved bulk microphysics scheme. Part I: Description and sensitivity analysis. *Mon. Wea. Rev.,* **132,** 519–542.

Twohy, C. H., A. J. Schanot, and W. A. Cooper, 1997: Measurement of condensed water content in liquid and ice clouds using an airborne counterflow virtual impactor. *J. Atmos. Oceanic Technol.,* **14,** 197–202.

Woods, C. P., M. T. Stoelinga, J. D. Locatelli, and P. V. Hobbs, 2005: Microphysical processes and synergistic interaction between frontal and orographic forcing of precipitation during the 13 December 2001 IMPROVE-2 event over the Oregon Cascades. *J. Atmos. Sci.,* **62,** 3493–3519.

Wurman, J., J. Straka, E. Rasmussen, M. Randall, and A. Zahrai, 1997: Design and deployment of a portable, pencil-beam, pulsed, 3-cm Doppler radar. *J. Atmos. Oceanic Technol.,* **14,** 1502–1512.